P'cabin

Edinburgh Wave Power Project

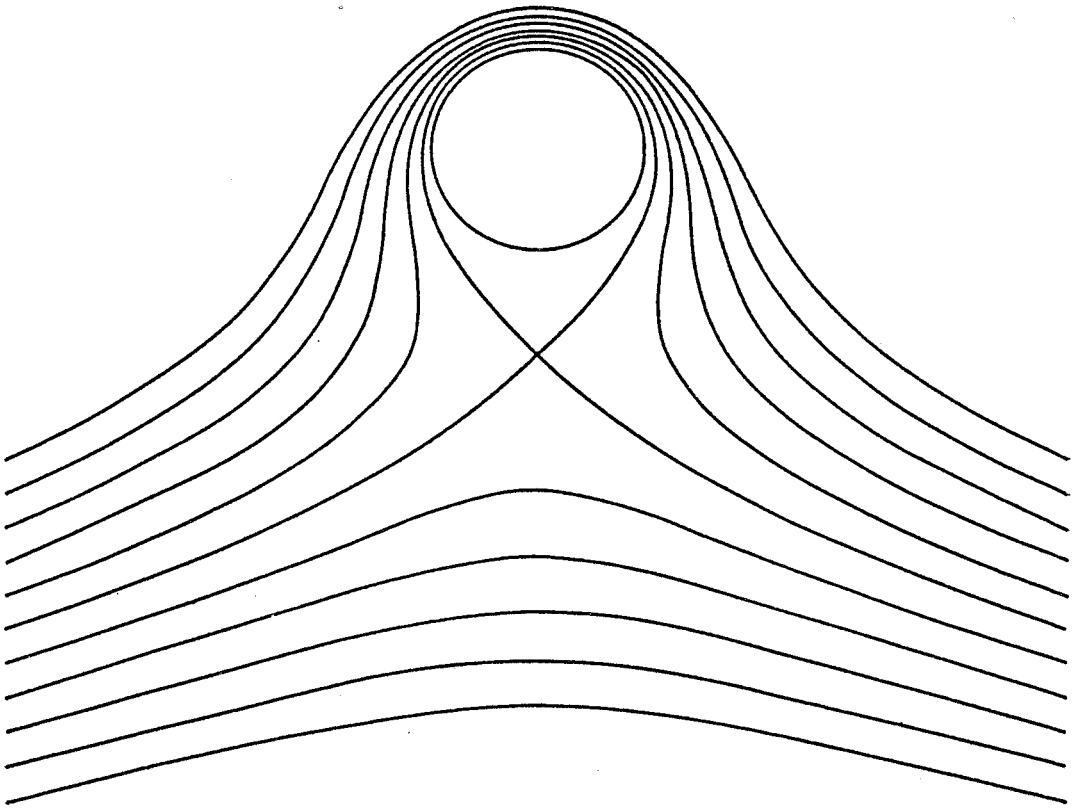

A Spinning Cylinder in Waves

1987

A SPINNING CYLINDER IN WAVES

A PRELIMINARY INVESTIGATION OF THE MAGNUS-BUDAL EFFECT

SERC Grant Number GR/D/8425.2

C H Retzler

July 1987

EDINBURGH UNIVERSITY WAVE POWER PROJECT
University of Edinburgh
Mayfield Road
Edinburgh EH9 3JL
031 667 1081 X 3276

CONTENTS

BACKGROUND

The Magnus effect is observed when an object possesses both rotation and translation relative to a fluid. The velocity of the object boundary relative to the fluid is the vector sum of the rotation and translation, and varies around the circumference. This velocity variation produces a Bernoulli pressure difference across the object towards the higher velocity, at a right-angle to the translation.

Applications have included the 'Flettner' rotor for sailing ships (the action of wind on two upright rotating cylinders allowed steering and propulsion); and the 'Towfish', a towed submersible for trawler net inspection (horizontal rotors produced lift and diving force).

Budal (1985) noted that an analogous phenomenon occurs in waves. In deep water, particles acted on by waves move in circular orbits; water particles at any point have vectors for velocity and acceleration which rotate in quadrature. The vectors produce drag and inertia forces respectively upon immersed objects. If a submerged cylinder is spun with its axis parallel to waves it will also experience a rotating lift vector in quadrature with the rotating velocity field. The lift vector therefore acts in line with the inertia force, and in phase or antiphase depending on the direction of spin.

Large lift forces are generated - a rotation rate equal to the wave frequency produces lift comparable with the inertia force. Therefore, by controlling the rate and direction of spin it is possible to increase, cancel or reverse the inertia force on a cylinder.

APPLICATIONS

We expect the Budal effect may be used to stabilise a variety of stationary or slow-moving vessels such as crane barges, semi-submersibles, and other vehicles associated with offshore industry. This will increase their operational weather window, and comfort for personnel.

The effect is realised by inducing a circulation, and although at model scale we are using a rotating cylinder to achieve this, at full size it may be more appropriate to use fluid emerging from tangential slots. Budal stabilisation would be particularly suitable for semi-submersibles, where the circulation could be induced around the submerged horizontal members, thus making a double use of the construction. Only a small power input would be required to maintain the circulation. Because the correcting forces are generated by the waves themselves the response is immediate and the energy expenditure is low, thus comparing favorably to dynamic positioning techiques.

CONCLUSIONS

1) Spinning a cylinder in waves can dramatically affect the force experienced by it. Spinning the cylinder in the same direction as the water orbitals can reduce, cancel, or even reverse the force. Spinning in the opposite direction can greatly increase the force.

2) We define positive cylinder spin to be in the opposite direction to the water orbitals; negative spin as the same direction. For a given spin rate, positive spin produces a greater force change than negative spin.

3) Graphs of force factor against spin factor show three distinct regions.
   a) A central region for small values of spin which has a steep slope. The slope extends further for positive spin than for negative.
   b) An upper region for positive spin which features reduced slope.
   c) A lower region for negative spin of slope slightly less than in (b).

4) The additional forces on the cylinder are related to spin speed and local fluid velocity. The vertical force shows good correlation with horizontal fluid velocity, and the horizontal force with the vertical velocity.

5) As wave frequency increases, the forces tend to decrease.

6) As cylinder axis depth increases, the forces reach a shallow maximum at a depth of about three and a half cylinder radii.

7) As wave amplitude increases, the forces reach a pronounced maximum when the amplitude approximately equals a cylinder radius.

8) It is well known that a fixed submerged horizontal cylinder causes a phase lag in a wave passing over it. We found that spinning the cylinder substantially changes this lag, and noted that the effect:
   a) is linear with spin factor until wave amplitude becomes comparable with cylinder radius;
   b) increases as the cylinder approaches the surface;
   c) is proportional to the cube of wave frequency.

APPARATUS

For this project we constructed a spinning cylinder rig, which we tested in our Narrow Tank. The cylinder rig consists of: a force sensing rig; an outrigger which supports and spins a cylinder; and associated electronics. The rig was designed for wide range and insensitivity to offset loads, easy change of models, and it was stressed for larger models to be tested in our Wide Tank. Photographs of the rig appear in the next section, together with constructional details. The material used is light alloy, except where otherwise specified. The principle of the rig is described briefly below.

The force rig

This has a space-frame construction enclosing two force-measuring modules. Each consists of a parallelogram linkage which is rigid to all forces except shear in one plane. This shear motion is constrained by a lever which bears upon a load cell. We use proprietory load cells supplied by RS Components, specified in Appendix 1. They have a range of +/- 20 N, and a travel of +/- 0.5 mm. The levers have adjustable pivot points which allow a range of 25 N to 400 N. For all the experiments in this report the 100 N range was used, with a resolution of 2 mN. The two modules are connected in series so as to sense horizontal and vertical forces on the outrigger. The displacement is a negligible 1 micrometre per Newton. The rig has a resonance due to the coupling of its moving mass and the load-cell compliance: on the 100 N range it is around 40 Hz, and is critically damped by a dashpot.

The outrigger

Two plates hold the test cylinder in ball bearings in its centre and at one end. This allows an unobstructed view of the free end of the cylinder when it is immersed in our glass-walled Narrow Tank. The cylinder is made up of a shaft and sleeves which are concentrically clamped to it by collets. We will be able to use this same principle to build up larger cylinders for tests in our Wide Tank.

A DC electric motor drives the cylinder via a toothed belt and pulleys with a 2:1 gear-down. The cylinder spin speed is measured by a tachogenerator integrated with the motor.

The depth of immersion of the cylinder can be quickly adjusted by a lead screw.

The electronics

The circuit board is mounted on an alloy space-frame at the back of the force rig. It contains the necessary electronics to drive the motor and and process the load-cell signals. The circuit diagrams are shown on the following pages.

A single-chip power amplifier drives the cylinder in either direction at spins of up to 27 Hz. At this speed the motor power consumption is 4 W, in air or water. This was nearly all due to bearing and belt forces, and so unfortunately not useful for predicting full scale power requirements. The power amplifier is fed by a pre-amplifier which sums an external command voltage with the tachogenerator feedback signal, thus providing velocity feedback. This summed signal is rolled off at 24 dB per octave above 100 Hz to avoid a belt resonance at 300 Hz and a motor/tachogenerator torsional resonance at 750 Hz. Consequently a large amount of negative feedback is available for error correction, and the cylinder can be held to a constant spin with root-mean-square error noise of about 2 mHz.

One +/- 15 V regulator is dedicated to the power amplifier, and another for the rest of the signal circuitry. The +/- 5 Volt excitation for each strain-gauge is supplied by individual sub-regulators. Taking care with regulation helps protect against motor noise spikes being injected into the signal path.

The strain-gauge outputs are buffered by high-gain instrumentation amplifiers, followed by a switchable-gain stage, and a 20 Hz low-pass anti-aliasing filter. The tachogenerator signal, and the current through the motor are also buffered and 20 Hz filtered. All these signals are available at a ribbon cable socket on the board, which is connected to the sampling system.

THE MOTOR CONTROL CIRCUIT

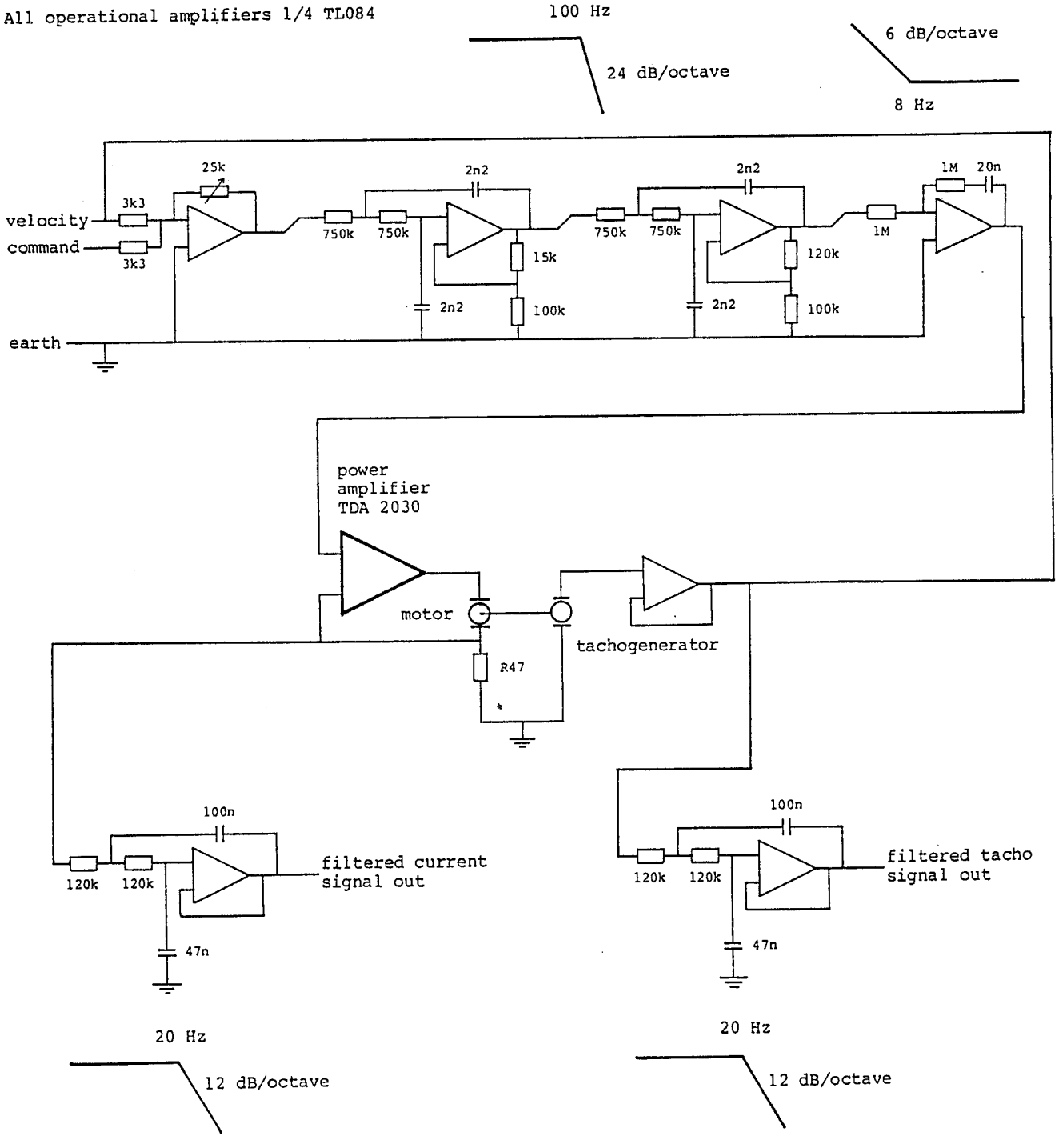

THE LOAD CELL CIRCUIT

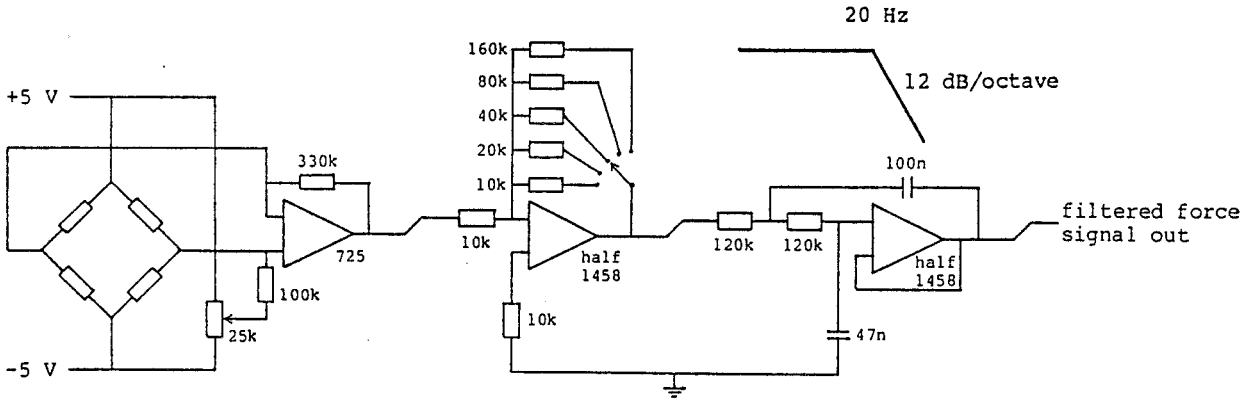

The Narrow Tank

This is a flume with interior dimensions: width 315 mm, height 725 mm, length 5.58 m. Water fills it to a depth of 580 mm. There is a wavemaker at each end. Either or both can be driven, both absorb unwanted waves. For these experiments just one was driven, producing simple travelling waves. In front of the other was placed an Expamet beach 1.8 metres long. This limited reflection to 1% between 1 and 2 Hz, rising to 9% down to 0.6 Hz. The frequency range is 0.2 - 3.0 Hz, although at high frequencies tank cross-waves corrupt the surface. A useful range is 0.5 - 2 Hz.

The sampling system

The sampling system consists of: a main computer, with direct memory access; a real time computer containing the master clock; and a sampling interface. The real-time computer generates waveforms to drive the wavemakers and the system under test (in this case the force rig). It also produces the sampling clock by dividing the master clock, and delaying it for a specified wait time.

The sampling interface, on receiving the clock signal, samples all the channels required by the main computer, scales them, and enters the results directly in main memory. Because signal generation and sampling are synchronised, all the waveforms can be made exactly periodic within the sampling interval. This has advantages for signal processing: for example, when a Fast Fourier Transform (FFT) is performed on the data, a spectrum is produced with a single tooth for for each frequency present in the sampled time series. If the bounds are aperiodic, smearing of the frequencies between teeth occurs.

Sampling parameters

The following sampling parameters were used for all the experiments described in this report.

Number of samples:	2048
Sampling rate:	80.0 Hz
Sampling period:	25.6 s
Sampling delay:	15.0 s

We chose 'integer frequencies' equal to n/25.6 Hz, where n is an integer. This ensured a whole number of wave cycles within the sampling period.

Photograph 1 The force rig and the outrigger

The outrigger is shown here in front of the force rig. It comprises:
a test cylinder consisting of a shaft, sleeves, and collets;
two support plates with press-fit ball bearings for the cylinder shaft;
a torque tube and two square spacer bars for the supports;
a motor, pulleys and toothed drive belt;
a lead screw, handle and flanged nut for height adjustment.

The test cylinder is shown at bottom left; its surface is polished smooth. It is held by the parallel support plates. Their reference edges run along their lower right hand side; these clamp to the face plate of the force rig. The reference edges of the support plates were milled, and the plates bored, while clamped together. Thus, when assembled, the bearings for the cylinder are exactly aligned. The collet arrangement which grips the cylinder is seen recessed in the nearer support. The motor is clamped to the further support and the pulleys and belt are recessed in its far side so as to present no additional frontal area to the waves.

Directly above the motor is the torque-tube, which prevents the outrigger assembly from twisting and so misaligning the bearings. It is thin walled to reduce unnecessary mass. The cap and bolt visible on this side of the left support are duplicated on the far side of the right support.

The outrigger is assembled on a surface table. The ball bearings are pressed into the bored recesses. The torque-tube is placed between the support plates and the two square spacer bars are screwed into place. The reference edges of the supports which clamp to the face plate of the force rig are pressed on the table, and the torque-tube is tightened. The stainless-steel shaft of the cylinder is then gently slid into the ball bearings, the alloy sleeving slid over it and the collets tightened. The cylinder spins freely, with a small clearance between it and the supports.

To adjust the depth of immersion of the cylinder in the water, the faceplate clamps of the force rig are loosened, letting the outrigger slide freely. The flanged nut is coned so that the outrigger can drop smoothly into place with the flange engaging with the top of the face plate. One of the four flats will stop the nut rotating. The lead screw is then turned to set the height.

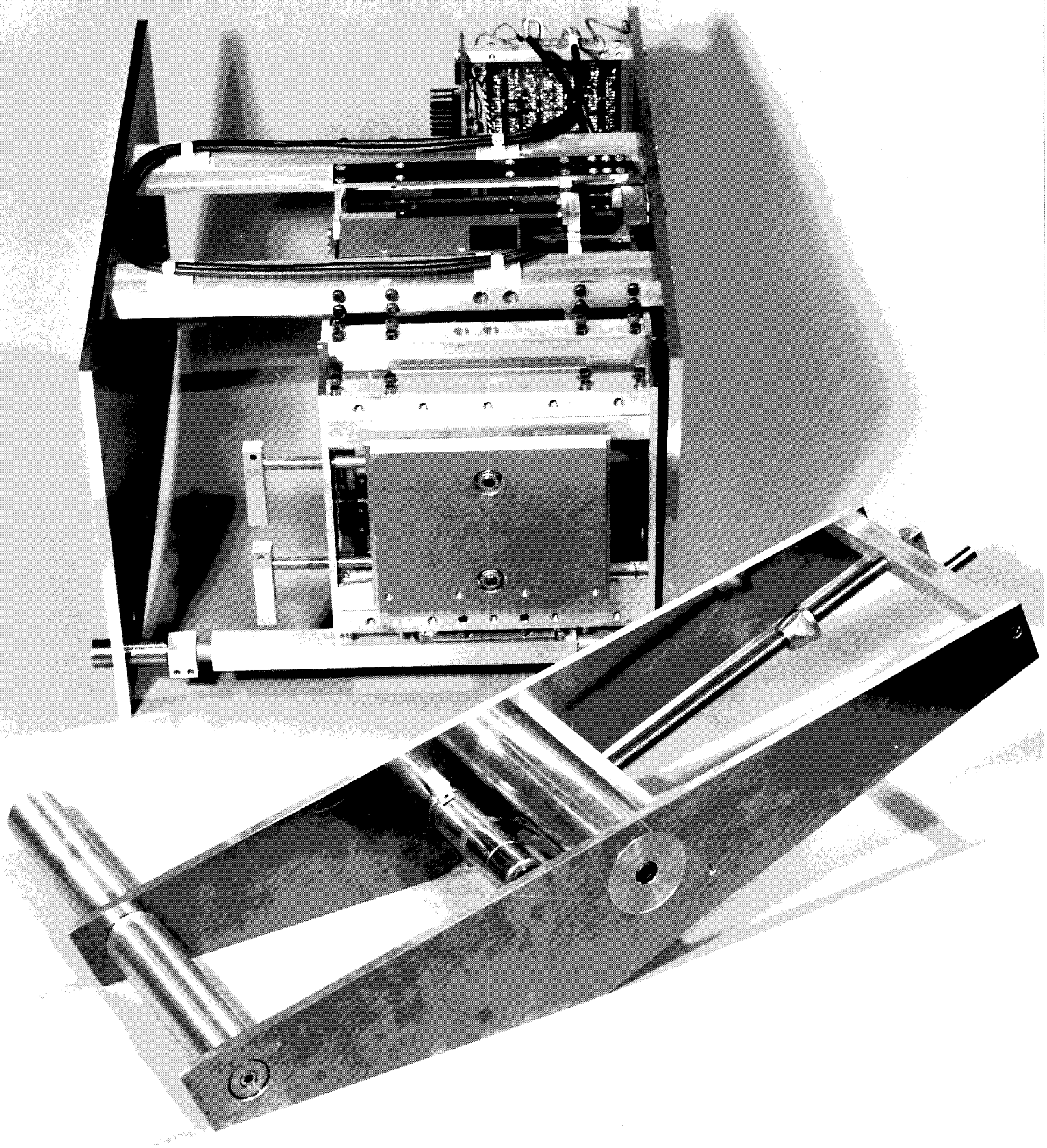

Photograph 2 The force rig

The two side plates are spaced by stainless-steel bars between their bottom corners at front and rear. Spacing the plates at the top are two pairs of square bars which support the force-measuring assembly. A pair of cables run along these bars from the circuit board at the back of the rig to the RS load cells, one of which can be seen nested within the cable run. This is for measurement in the horizontal direction. Its base is bolted to the bar; its force bearing surface at the top left pivots on a space-frame lever, whose fulcrum is at the side plate at the right. Between them is the pivot where the lever attaches to the moving rig. All the pivot points are leaf springs in order to provide zero stiction, made of fatigue-resistant beryllium-copper.

The vertical parallelogram assembly is at the front of the rig, and is similar in principle to the horizontal one. A pair of square bars are clamped with a stee; leaf spring between them at each end. Another pair of bars clamps the other ends of the springs. This arrangement is visible at the front of the photograph: the springs appear as black strips; the four Allen screws at each end of the pairs of bars provide the clamping force. The arrangement is copied beneath to form the other arm of the parallelogram. The four front bars are held rigidly together by side plates, as are the rear four; the whole assembly thus forms two planes which are rigid in every degree of freedom except parallel shear. The assembly resisted a compressive load on the front face of more than 1200 Newtons, three times the maximum measurement range, without buckling failure. The front surface of the bars has been milled flat to provide a bearing surface for the outrigger to be clamped against. In addition, the top and bottom bars have each been drilled and tapped in five places to allow other items to be attached if ever required.

The face plate is at the very front of the rig. Its flanged sides engage with slots in the support plates of the outrigger. The nuts in the middle of the plate provide fine adjustment of two stainless-steel camshaft assemblies which are turned by the levers visible at the left, to clamp the edges of the outrigger support plates firmly against the bearing surface of the bars.

At the front of the rig, clamped to the steel stub supports with pinch blocks, is a damping trough filled with very high viscosity silicone oil. A paddle is bolted to the vertical parallelogram assembly, and sits in the fluid. The rig resonances are thereby critically damped horizontally and vertically.

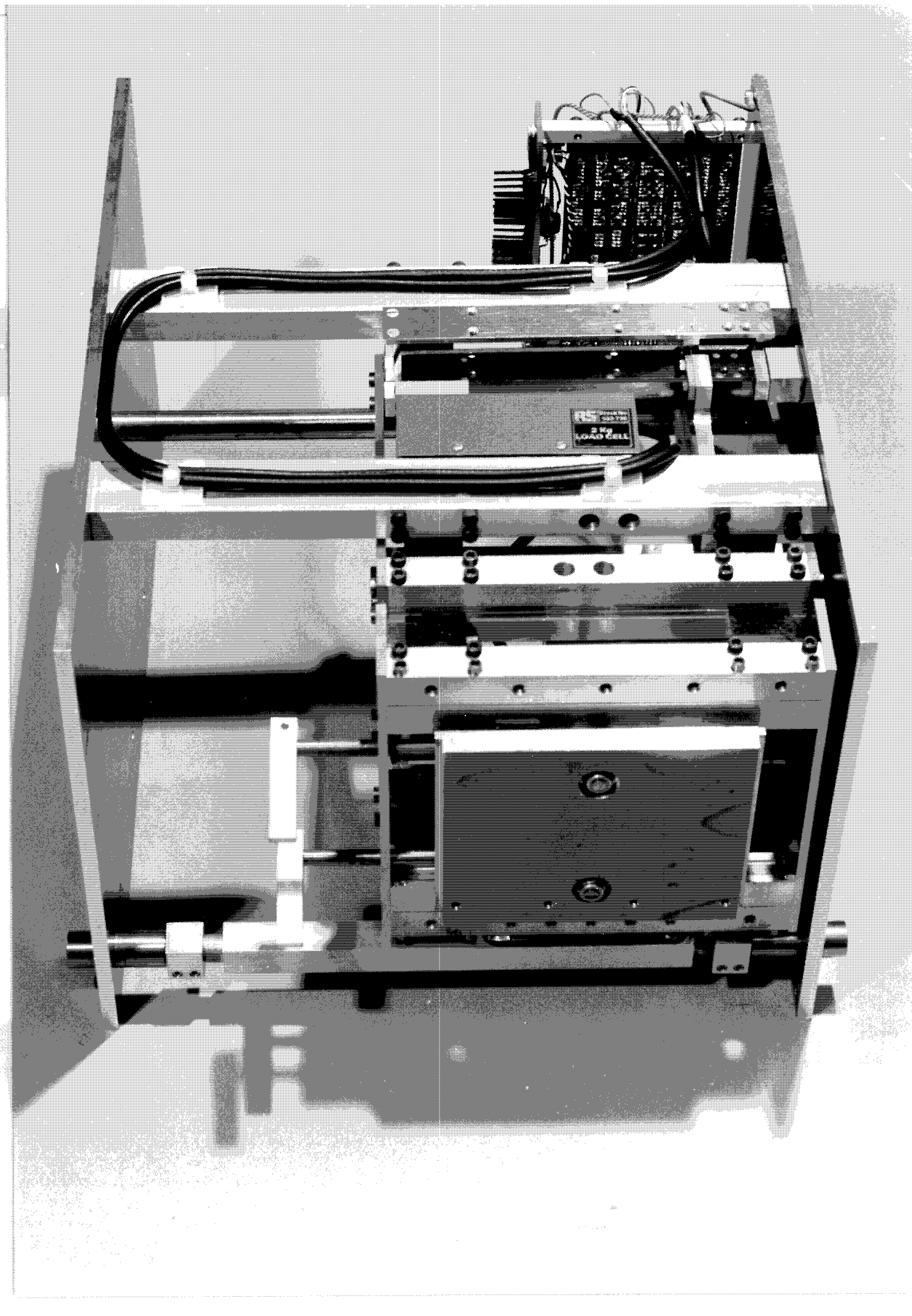

Photograph 3 The rig resting on the Narrow Tank

This view shows the rig resting on the horizontal rails of the wave tank. Clamping plates, not visible here, hold the rig side plates to the tank walls.

One can see that the toothed drive belt and the pulley on the cylinder are recessed into the support, and offer no additional obstruction to the waves.

The wires to the motor are visible passing over the top of the apparatus. In use, both the motor wires and the tachometer cable are arranged so that they rest loosely on the outrigger, so that their mass or tension does not corrupt the force signals.

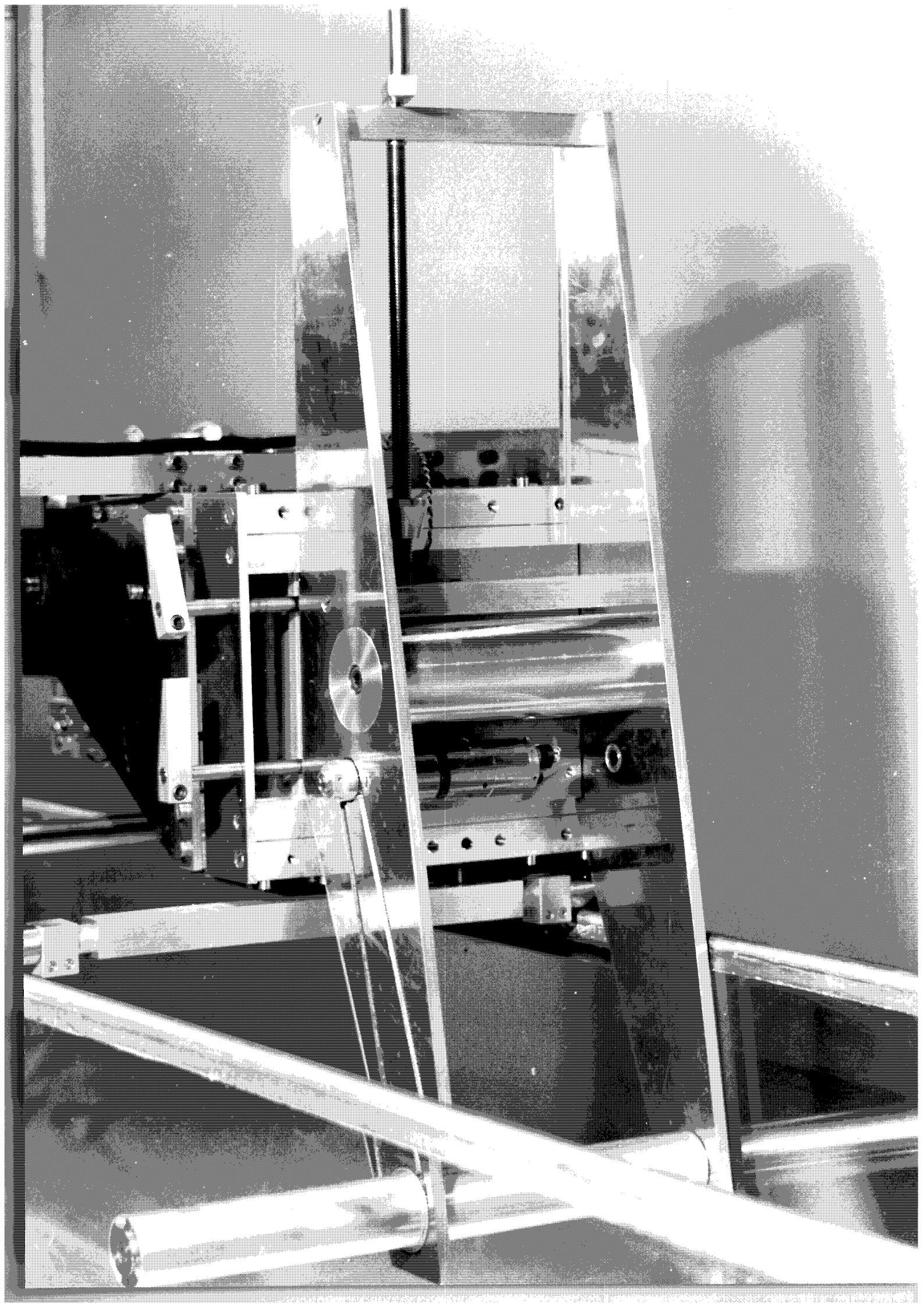

Photograph 4 The cylinder spinning in the water.

This view shows how the reference edges of the support plates press against the milled face of the vertical parallelogram assembly.

The belt is visible within its milled recess, driving the cylinder.

At the end of the cylinder, the collet detail is visible. The central bolt tightens the end-cap on the collet, compressing it against the coned inner surface of the sleeve, and tightening it around the shaft.

The wave is much larger than those used in the experiments, and consequently there is a lot of wave diffraction around the supports.

The wave is shown coming from the right, which we define as the positive surge direction.

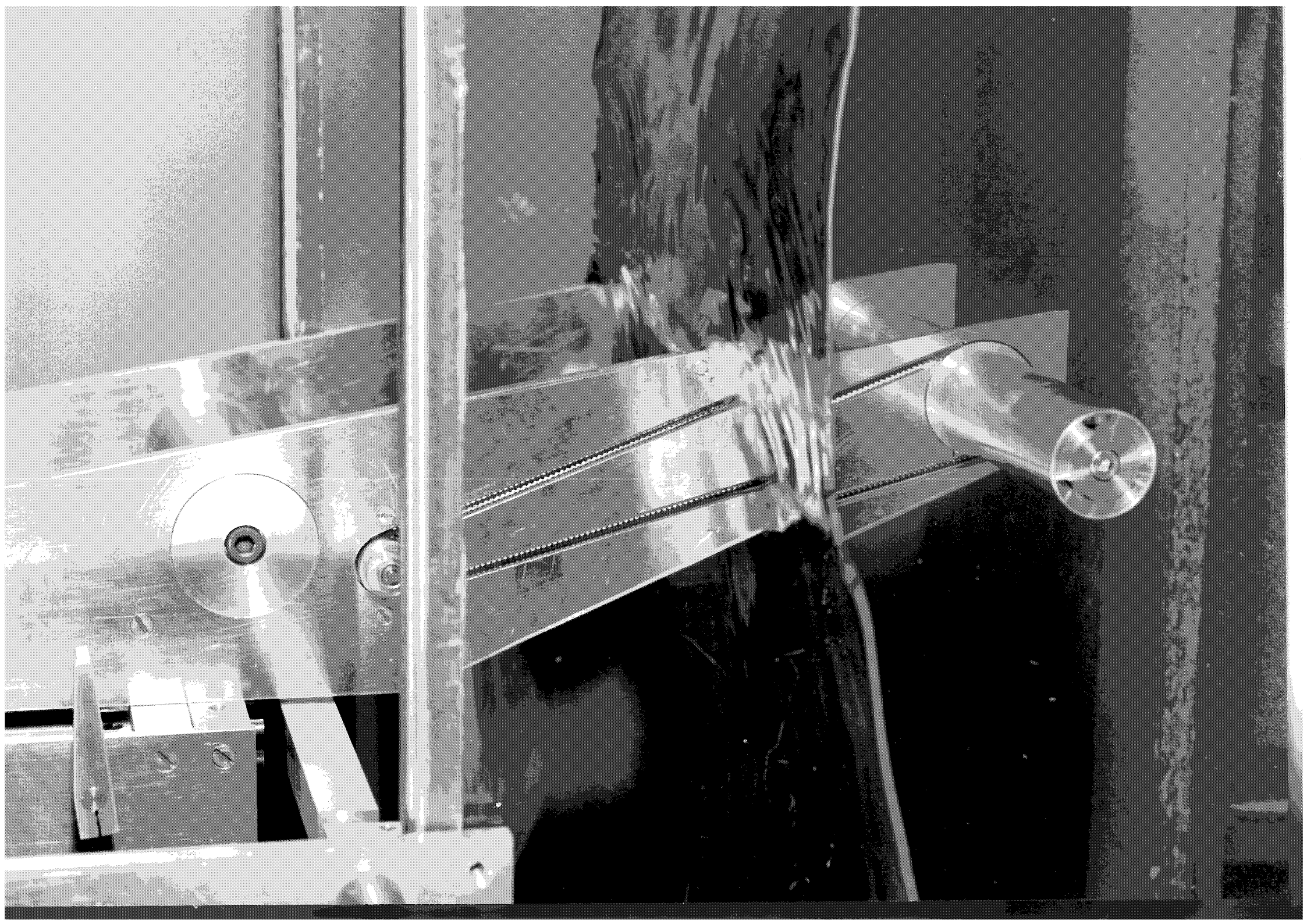

SCALING CONVENTIONS

In his 1985 paper, Budal developed an approximate theoretical expression for the waveforce on a horizontal submerged spinning cylinder. He showed that the force on a spinning cylinder parallel to the wave crests is related to the force on one at rest - the zero-spin force - by a factor $1 + \omega_r/\omega$ where ω_r and ω are respectively the angular frequencies of the cylinder and the wave. His experiments showed that the force on the cylinder could indeed be considerably increased or decreased by spinning it, although the agreement with theory applied only over a limited spin range.

In this work we retain the concept of measuring a force factor and a spin factor which we define as follows:

$$\text{spin factor} = \frac{\text{angular frequency of cylinder}}{\text{angular frequency of wave}}$$

$$\text{force factor} = \frac{\text{force on spinning cylinder - zero-spin force}}{\text{zero-spin force}}$$

We define the spin factor as positive when the cylinder spins in the opposite direction to the wave orbitals: negative when it spins in the same direction. The force factor differs from Budal's in that it is additional force, not total force, that is compared with the zero-spin force. Note that the force is complex: it has both magnitude and phase. The above expression for the force factor is therefore in complex arithmetic, and yields as its real and imaginary parts the extra force due to spin, in phase and quadrature, scaled by the zero-spin force.

The justification for scaling by the zero-spin force is that it provides a reference. It allows one to see at a glance how much force is generated, and whether force cancellation is possible.

The disadvantage is that the zero-spin force is the resultant of inertial and drag forces. It would be satisfying to use the wave itself as the reference; to relate the force on the cylinder to the complex amplitude of the wave at the position of the cylinder: then complex division of the force by the amplitude would yield the inertial and drag forces separately. However, when we tried this approach, the results were inconsistent because of the extent to which the presence of the cylinder alters the wave field.

THE EXPERIMENTS

The cylinder used throughout these experiments has the following dimensions:

Length	290.0 mm
Radius	17.0 mm
Volume	263 millilitres

The cylinder supports are 6.5 mm thick and taper in width, having a mean width of about 75 mm. Together they displace about 105 millilitres, when the cylinder is immersed to 100 mm. Most of the force on the cylinder is inertial and therefore proportional to volume. The cylinder supports will therefore have a substantial effect. In the following experiments the effects of the supports have, to a first approximation, been cancelled by re-running each experiment with the same parameters but with the cylinder removed, and just the supports left in place. The results for the supports alone are then subtracted from the composite results to yield data for the cylinder alone.

Our experiments covered a range of of wave amplitude and frequency, depth of immersion of the cylinder, and cylinder spin ratio. The latter had the same range in each experiment, namely -9.8 to +9.8 in steps of 0.02. Each experiment included the reference case of the cylinder at 100 mm depth, wave frequency 1.016 Hz, and wave amplitude 10 mm. These values were set by the following considerations.

Tank reflection: Reflection from the beach is lowest around 1 Hz. The closest 'integer frequency' to this is 1.016 Hz.

Surface effects: From graphs given by Ogilvie (1963) the water surface has negligible effects on the cylinder at depths of 5 times the radius. This corresponds to 85 mm.

Keulegan-Carpenter number: $K_c = \frac{U}{2fr} = \frac{\pi a}{r}$

U = water orbital velocity
f = wave frequency
a = water orbital amplitude
r = cylinder radius

Chaplin (1984) observes that wake-separation, and considerable vortex-shedding will occur for $K_c > 2$. For this cylinder, at a depth of 100 mm, in a 1.016 Hz wave of 10 mm surface amplitude, we obtain $K_c = 1.22$, well below the limit.

Two wave gauges were placed 600 mm fore and aft of the cylinder. The apparatus was calibrated and the results loaded into scaling files. In all the experiments the following data were collected:

cylinder spin rate	Hertz
heave and surge forces on the cylinder	Newtons
wave height	metres

While every effort was made to reduce extraneous sources of noise - mains hum, amplifier noise, rig vibration, cylinder vibration due to the toothed belt drive - we took the precaution of Fourier filtering. Only data at the same frequency as the specified wave frequency were retained. Regrettably, while this removed most noise, it also threw away potentially interesting harmonic information, of relevance to non-linear effects. However, for the 'reference case' of a 1 Hz wave, amplitude 10 mm, cylinder depth 100 mm, the second harmonic content of force was about 1%, for a spin factor of 5. Higher harmonics were even less. This proportion is very low and very vulnerable to noise.

THE GRAPHS

The twelve pages of graphs which follow show results for three experiments:

1) **Six cylinder axis depths:** 40 mm to 140 mm, in steps of 20 mm.
   Wave frequency 1.016 Hz, wave amplitude 10 mm.
   Spin factor -9.8 to +9.8 in steps of 0.02. 99 values total.

2) **Six wave frequencies:** 0.63 Hz to 1.6 Hz, in steps of 0.195 Hz.
   Wave amplitude 10 mm, cylinder axis depth 100 mm.
   Spin factor -9.8 to +9.8 in steps of 0.02. 99 values total.

3) **Six wave amplitudes:** 5 mm to 30 mm, in steps of 5 mm.
   Wave frequency 1.016 Hz, cylinder axis depth 100 mm.
   Spin factor -9.8 to +9.8 in steps of 0.02. 99 values total.

On each page are six graphs of force factor against spin factor, one for each value of the changing parameter.

The results for each experiment consist of a set of four pages of graphs. These show the force factor in phase and in quadrature with the zero-spin force for heave and surge.

The fixed parameters are specified at the top of each page, and the changing parameter at the top of each graph box. The axes of all the graphs are: force factor vertical, spin factor horizontal; the same scales are used throughout. A continuous line joins the 99 datum points. Because of the definition of force factor, it equals zero when the spin factor equals zero. Each line therefore necessarily passes through its graph origin.

At the bottom of each graph box the zero-spin force is shown. Multiplying this by the force factor at any spin factor gives pure force. Comparing zero-spin forces for the reference case in each of the three experiments shows a repeatability of +/- 3%.

Cylinder depth

Considering heave and surge in-phase results:

1) Heave and surge graphs are very similar: at each depth, the same features appear in each. The surge zero-spin forces are slightly lower, and the surge force factor curves also have very slightly less slope.

2) The zero-spin force decreases with depth, due to the decreasing size of the water orbitals.

3) The values of force factor for negative spin remain similar for all depths.

4) For positive spin, the force factor curves change noticeably and steadily with depth. The greater the depth, the lower the slope of the curves; also the less the extent of the higher-slope central section.

5) The graph for the shallowest depth, 40 mm, differs from the rest in showing a pronounced curve in the higher spin regions. This may be related to an observation during the course of the experiment that at this depth cylinder spin caused acute distortion of the water surface, almost causing a breaking wave at the highest values of spin.

6) The scatter on the curves increases with depth. This is surprising: if if it were a hydrodynamic effect, one would expect it to be greater near the surface, where higher fluid velocities are more likely to cause vortex shedding.

Considering heave and surge quadrature results:

7) As positive spin increases the force factor remains close to zero. This means that though the magnitude of the force on the cylinder increases, its direction remains almost unchanged. This implies that inertial and drag components on the cylinder stay in almost equal proportion.

8) The force factor shows a steady slope with negative spin. We may surmise that this is due to the cancellation and reversal of the inertial force, while the drag force remains unaffected.

Figure 1a IN-PHASE HEAVE force factor against spin factor

Wave frequency = 1.02 Hz

6 CYLINDER DEPTHS

Wave amplitude = 10 mm

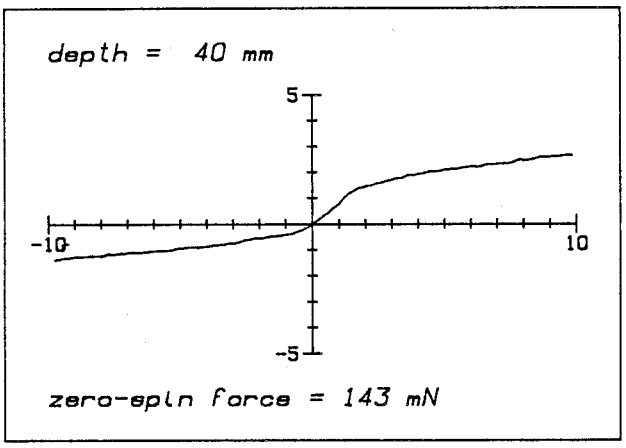

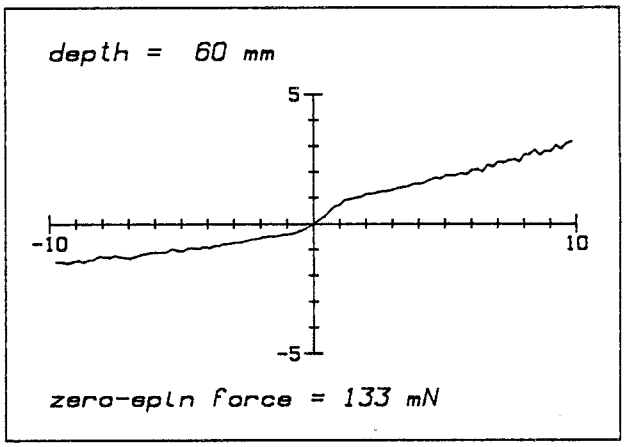

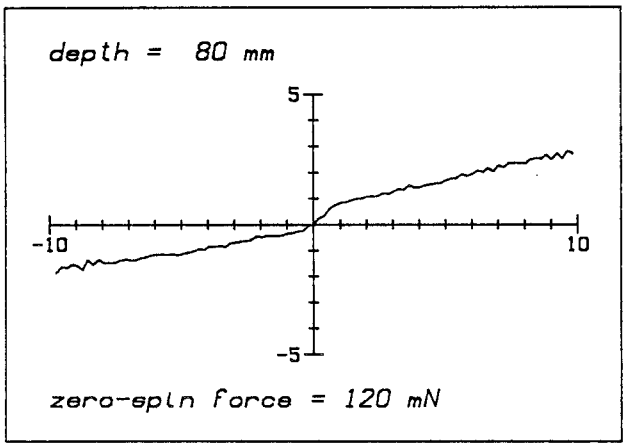

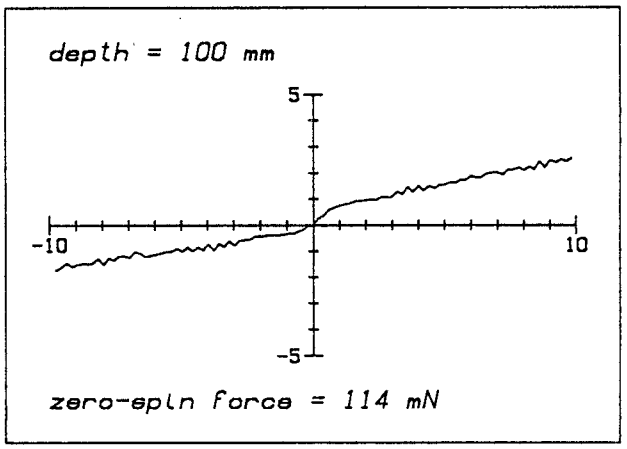

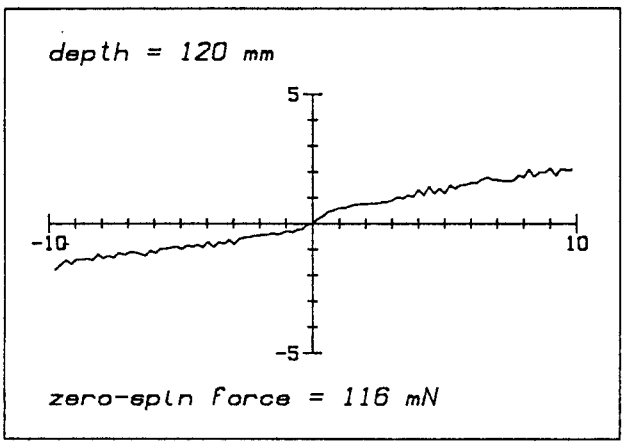

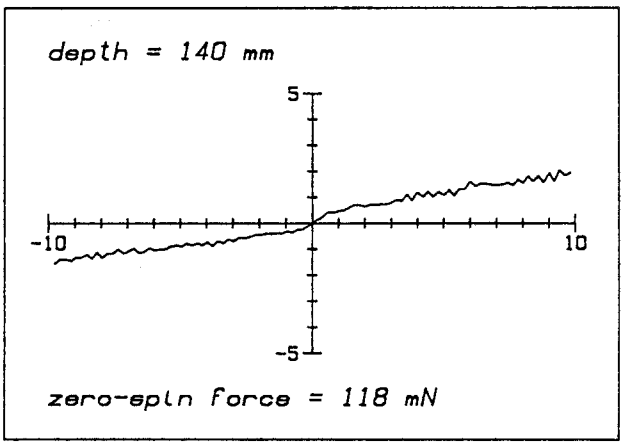

Figure 1b QUADRATURE HEAVE force factor against spin factor

Wave frequency = 1.02 Hz

6 CYLINDER DEPTHS

Wave amplitude = 10 mm

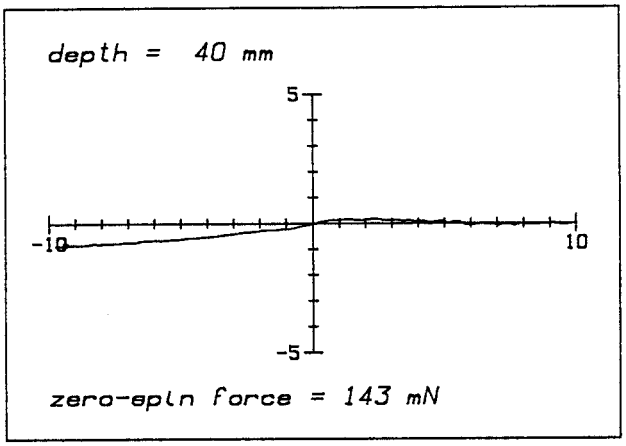

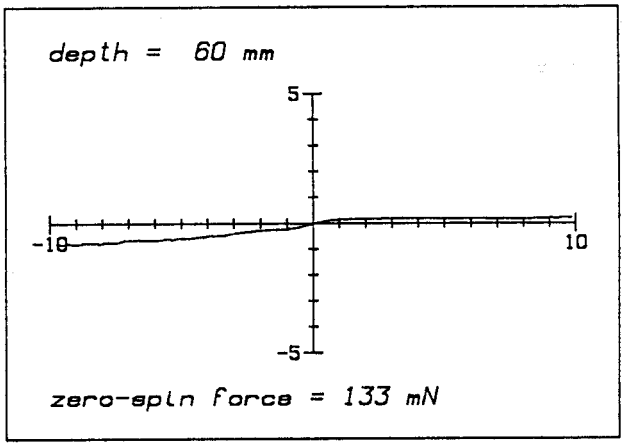

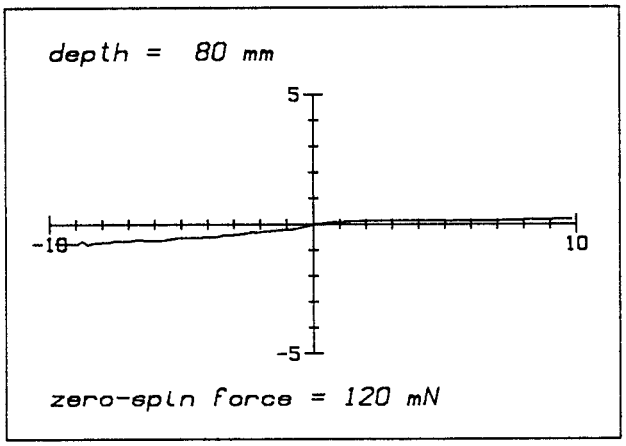

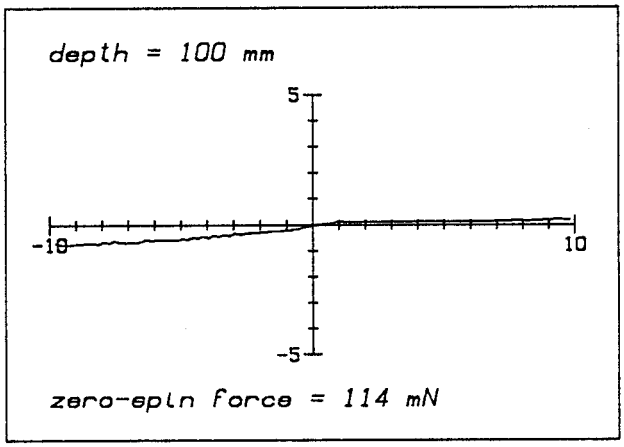

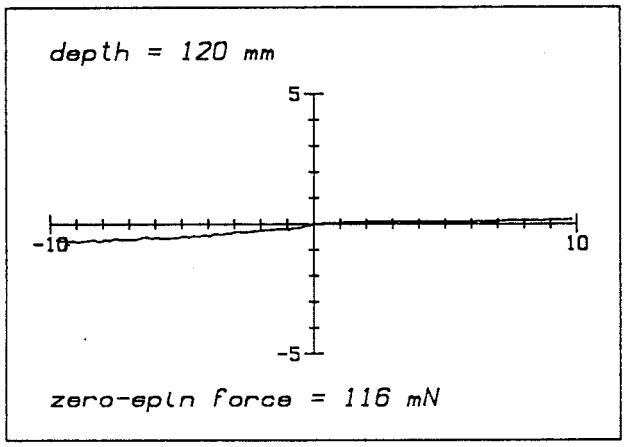

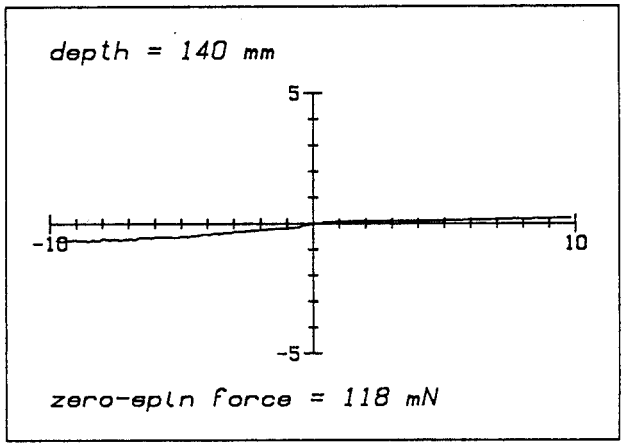

Figure 1c IN-PHASE SURGE force factor against spin factor

6 CYLINDER DEPTHS

Wave frequency = 1.02 Hz

Wave amplitude = 10 mm

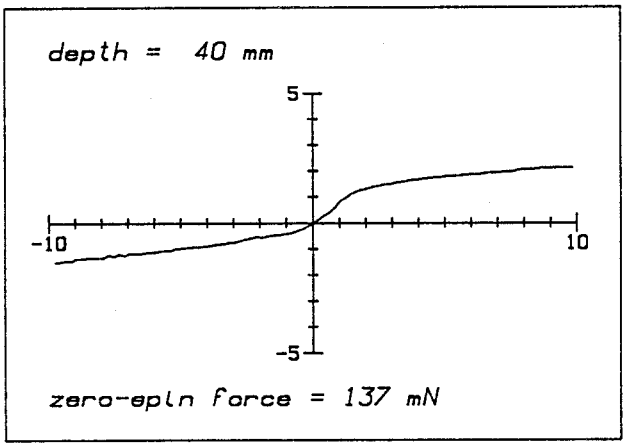

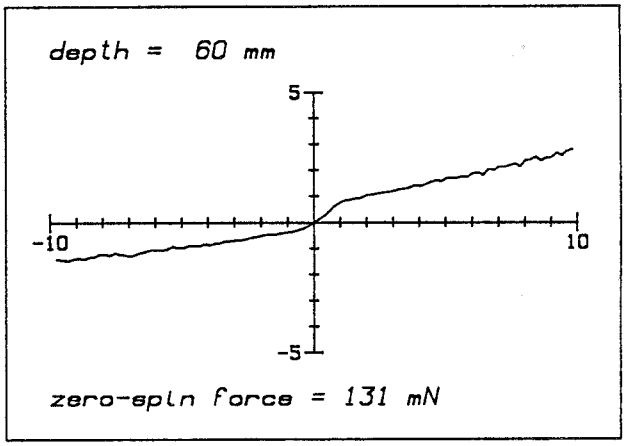

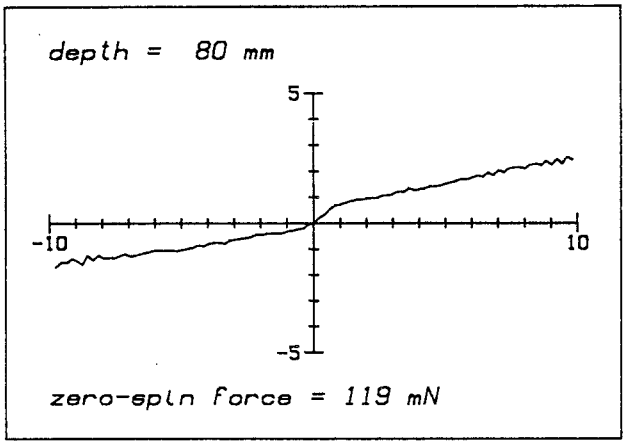

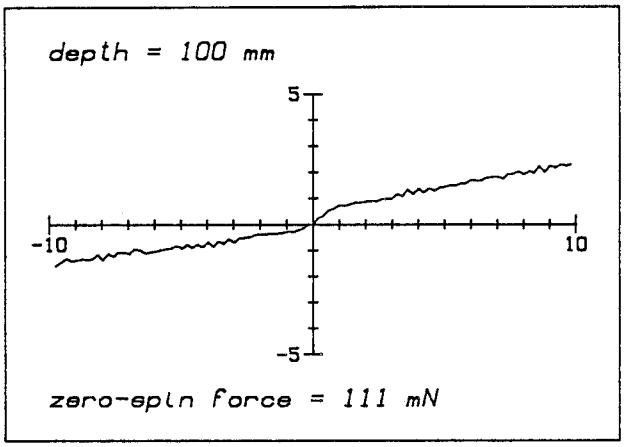

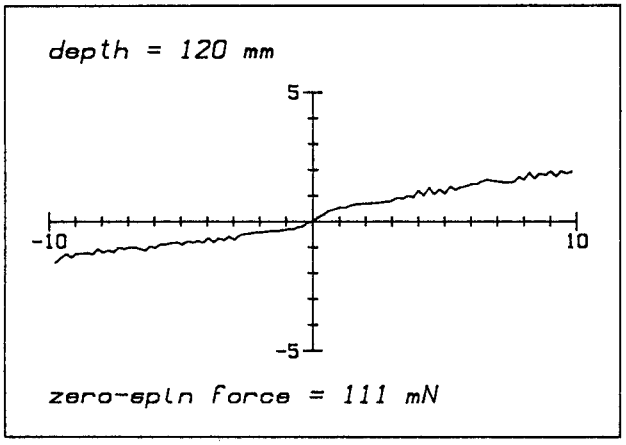

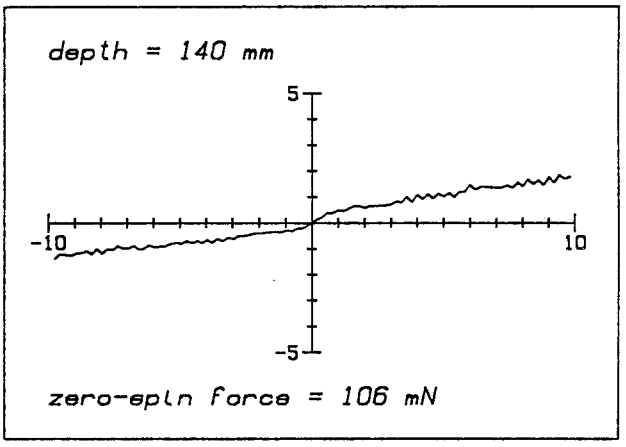

Figure 1d QUADRATURE SURGE force factor against spin factor

Wave frequency = 1.02 Hz

6 CYLINDER DEPTHS

Wave amplitude = 10 mm

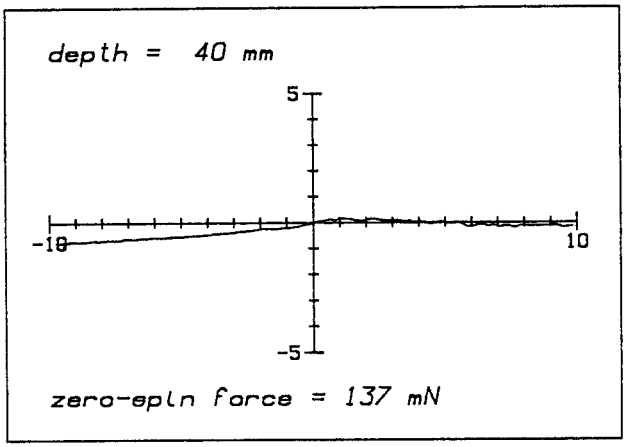

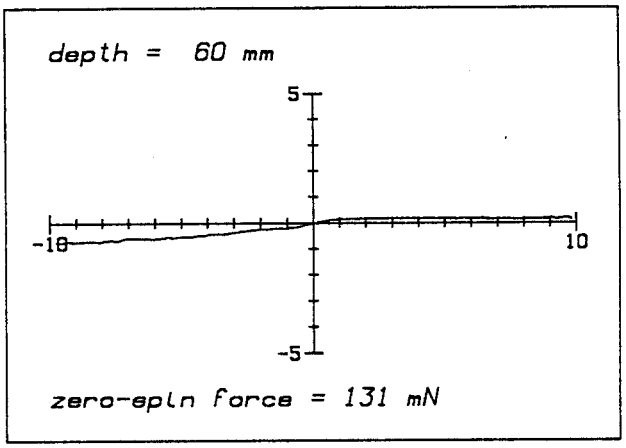

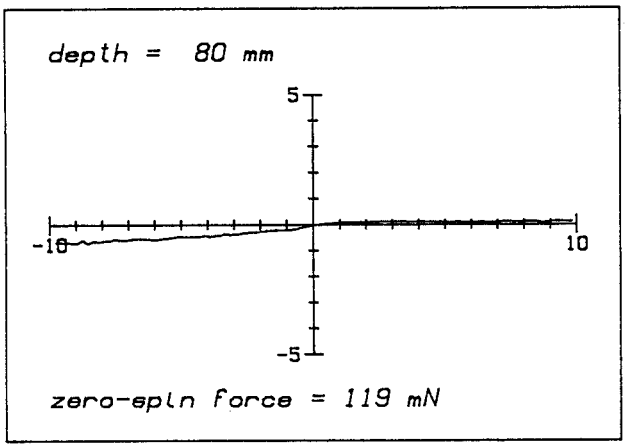

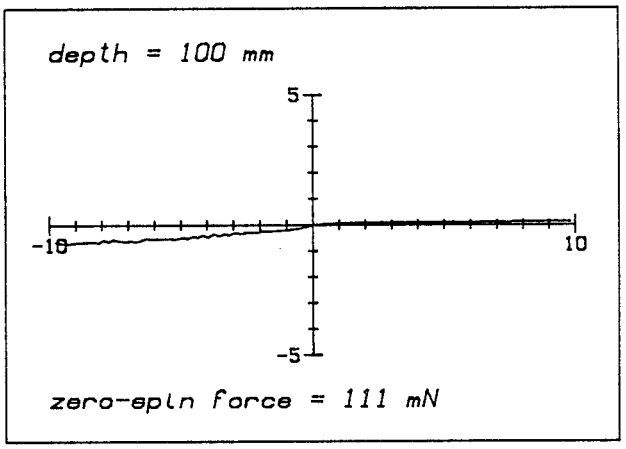

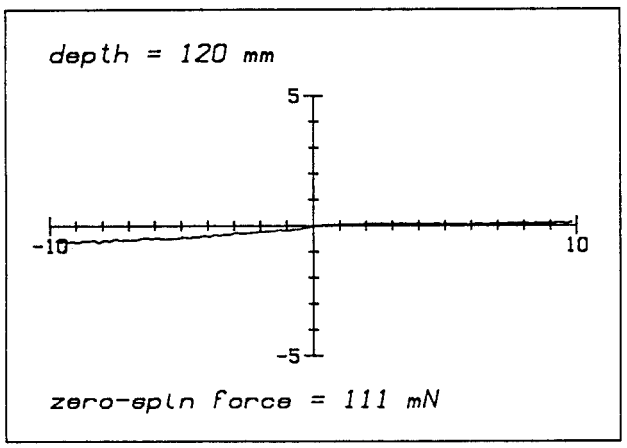

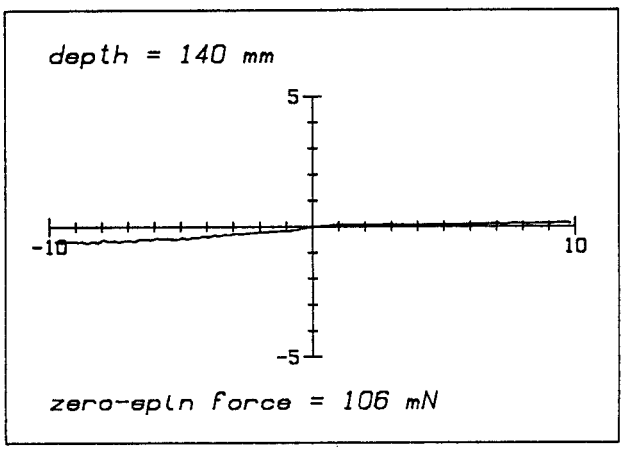

Wave frequency

Considering heave and surge in-phase forces:

1) Immediately apparent are the high heave force factors at 0.63 Hz. These arise because of the surprisingly low value of zero-spin force in heave.

2) The rest of the zero-spin forces, in heave and surge, show a steady increase with frequency, which is due to the greater acceleration of the water with wave frequency, partly offset by the more rapid decrease with depth in size of the water orbitals.

3) Force factors for positive spin show a steady decrease as frequency increases. Much of this is due to the decrease in extent of the central high-slope region. There tends to be less change for negative spin.

Considering heave and surge quadrature forces:

4) In surge, as positive spin increases, the force factor remains almost zero, implying that while cylinder force increases, it remains in the same direction as the zero-spin force. For negative spin, there is a steady change of force with spin, as the inertial force cancels but drag remains.

5) In heave, for the 0.63 Hz case, there is a large amount of 'spill-over' of the in-phase graph into the quadrature graph. This is a consequence of the unusually low zero-spin force which has been used as the reference. As well as being low, it will have a different phase, because of a different ratio of inertial to drag forces.

6) In heave, for other frequencies, there is more change of force factor for positive spin than in the surge case. This is most apparent at 0.82 Hz, and 1.60 Hz. It is a reminder that the choice of the force on the rest cylinder as the graph scaling factor was arbitrary, and there may well be some other reference which results in more consistent graphs.

Figure 2a IN-PHASE HEAVE force factor against spin factor

6 WAVE FREQUENCIES

Wave amplitude = 10 mm

Cylinder depth = 100 mm

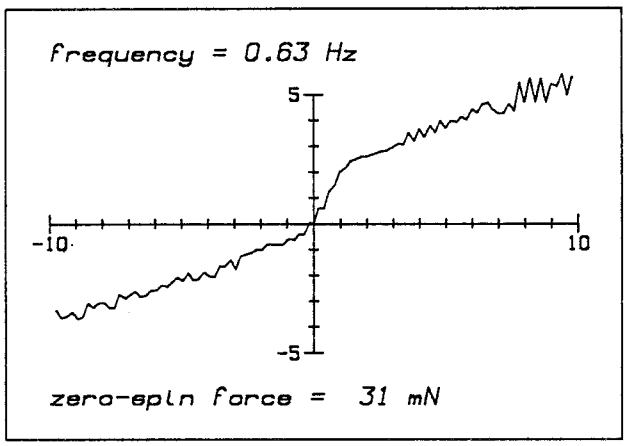

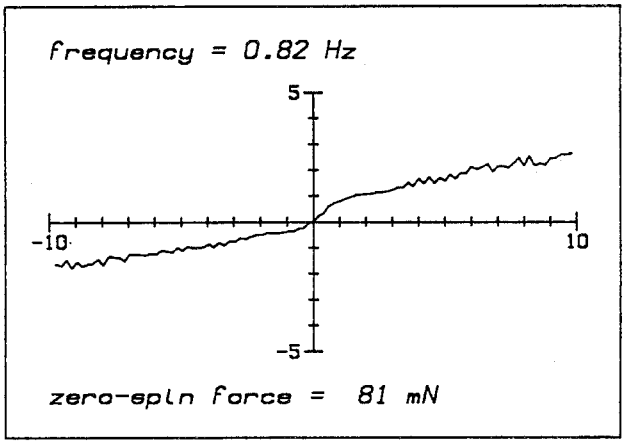

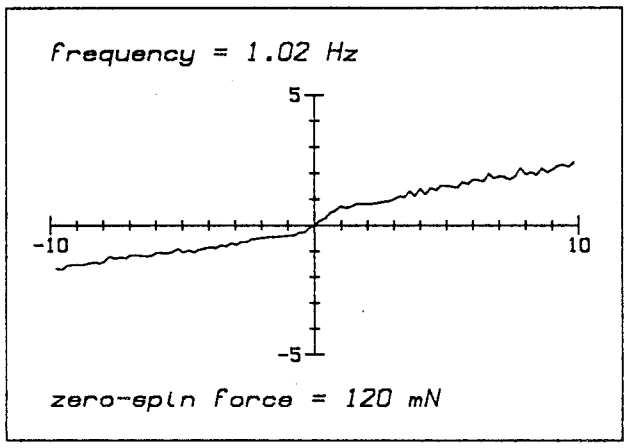

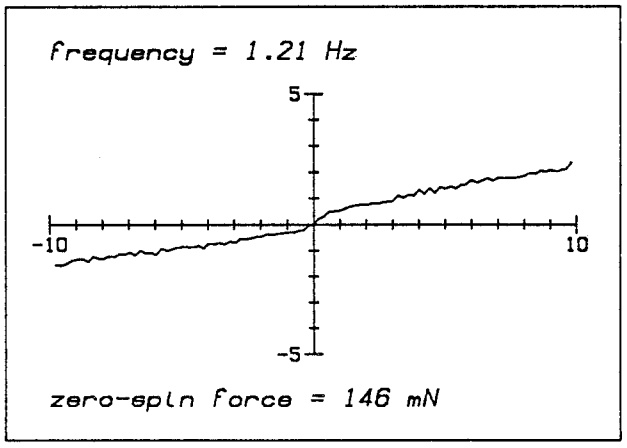

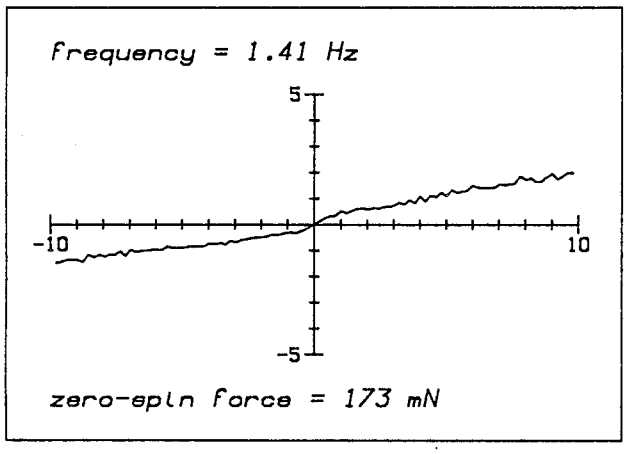

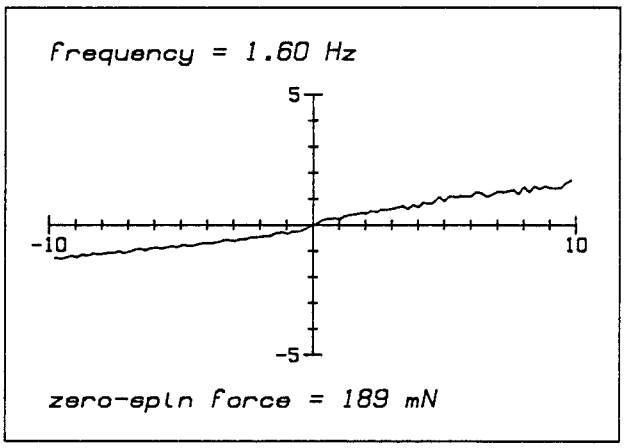

Figure 2b QUADRATURE HEAVE force factor against spin factor

6 WAVE FREQUENCIES

Wave amplitude = 10 mm

Cylinder depth = 100 mm

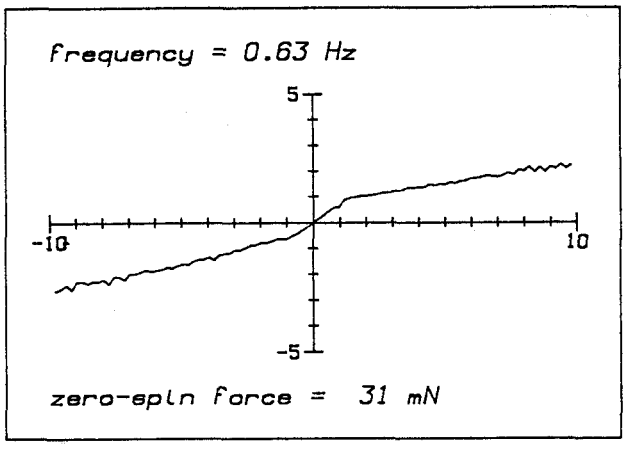

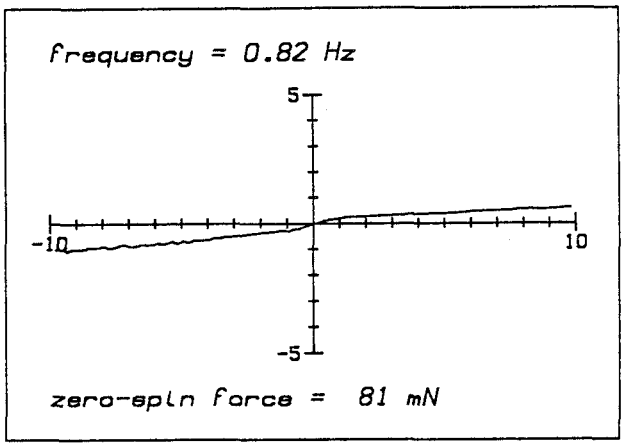

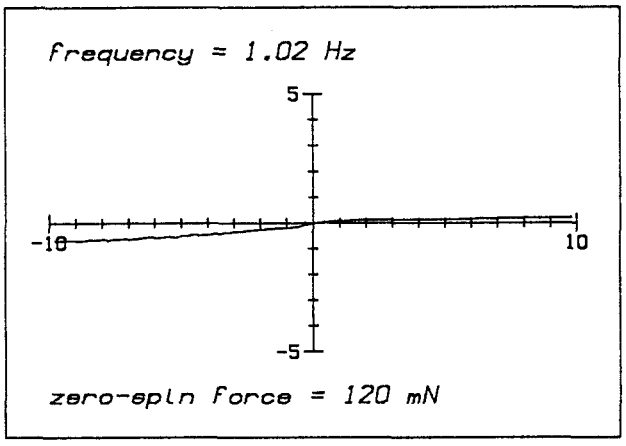

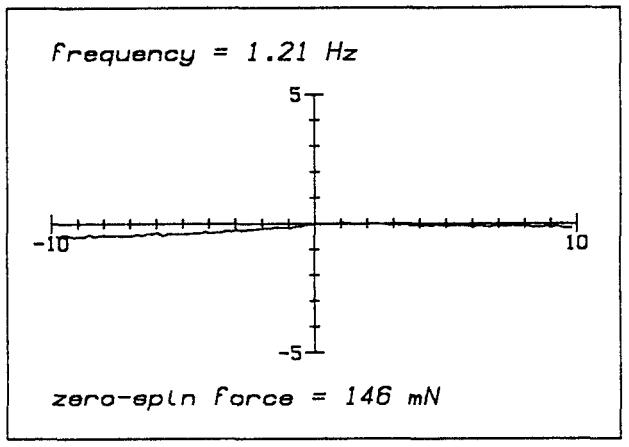

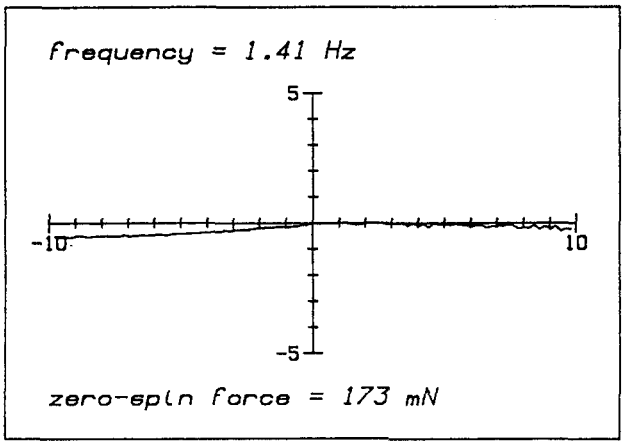

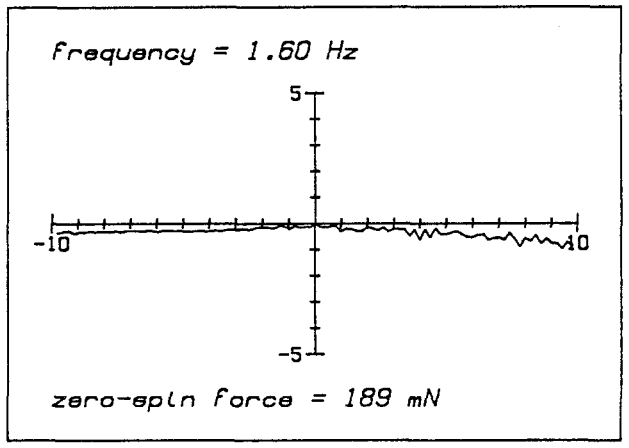

Figure 2c IN-PHASE SURGE force factor against spin factor

6 WAVE FREQUENCIES

Wave amplitude = 10 mm

Cylinder depth = 100 mm

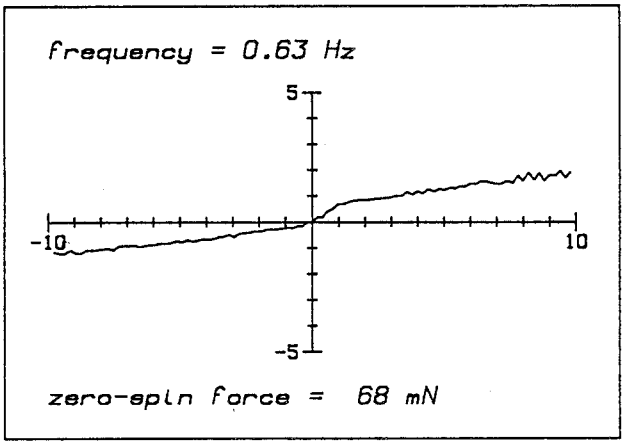

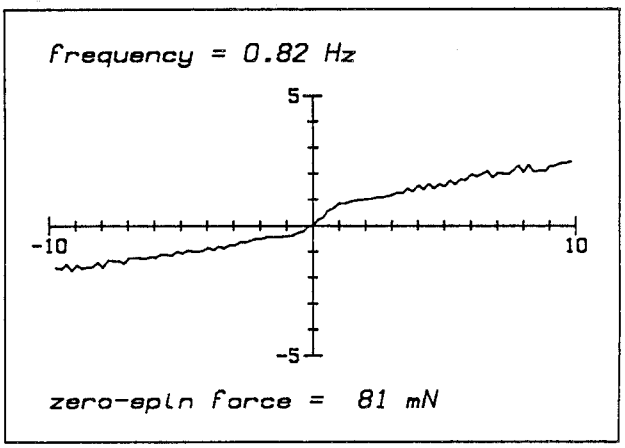

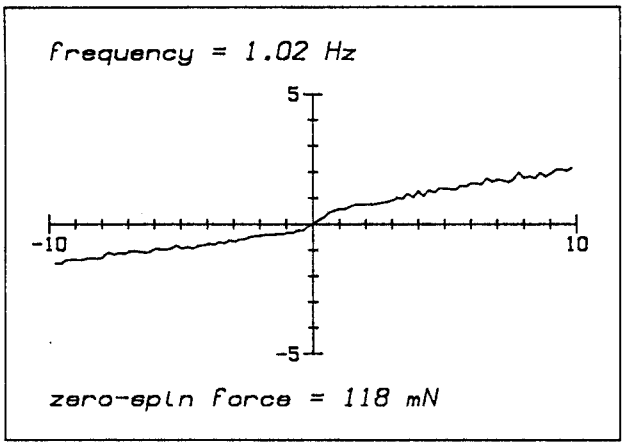

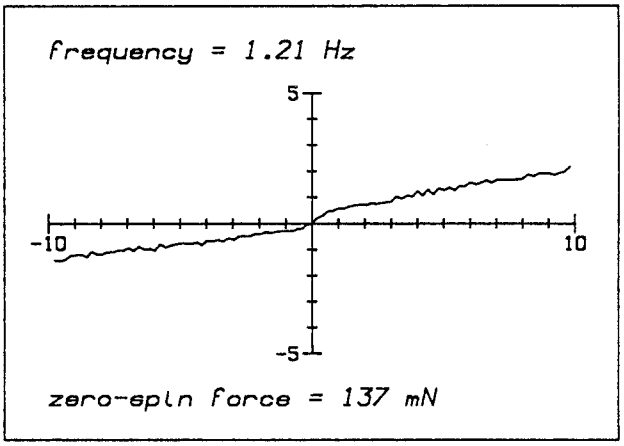

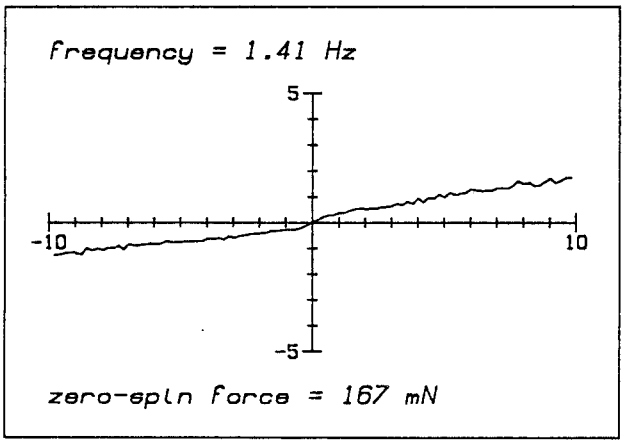

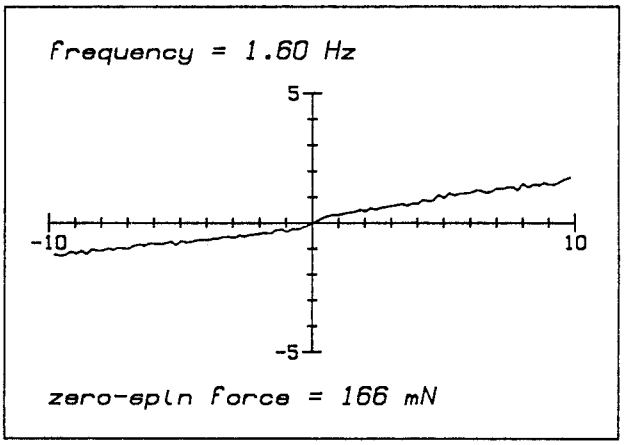

Figure 2d QUADRATURE SURGE force factor against spin factor

6 WAVE FREQUENCIES

Wave amplitude = 10 mm

Cylinder depth = 100 mm

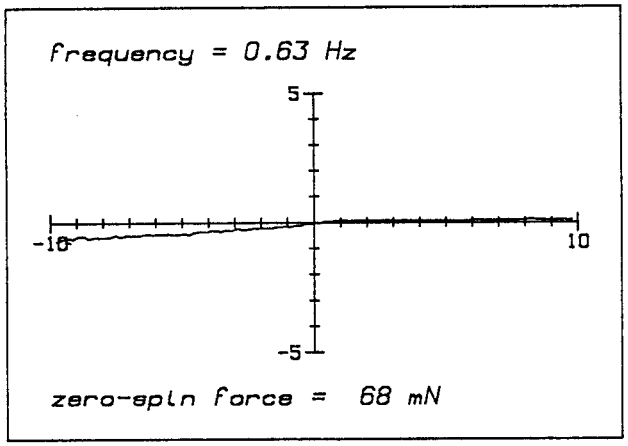

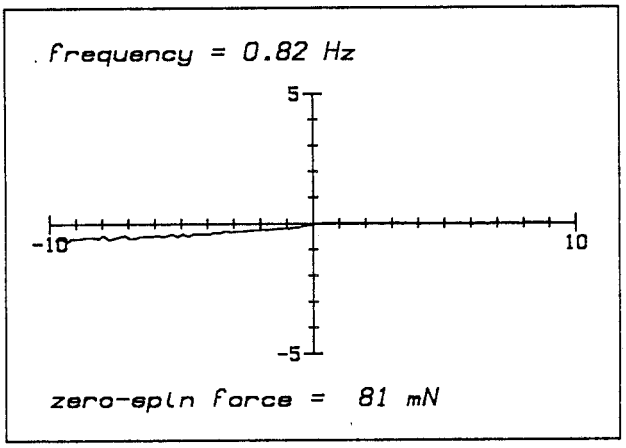

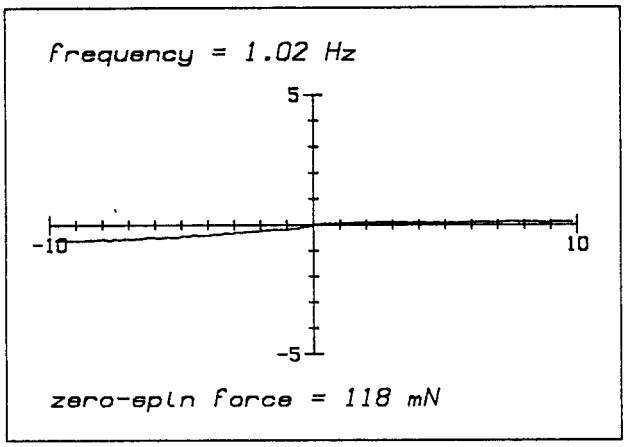

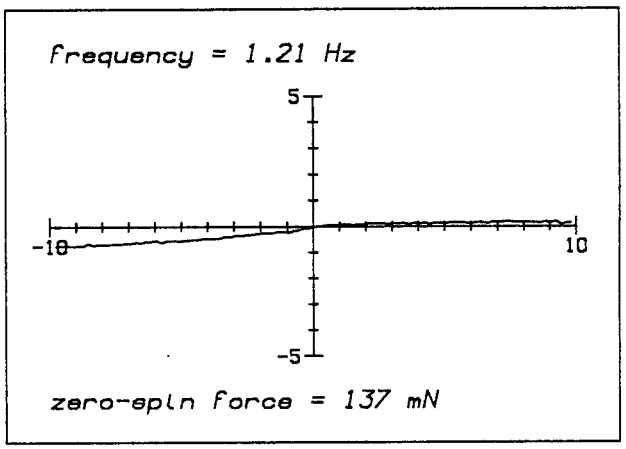

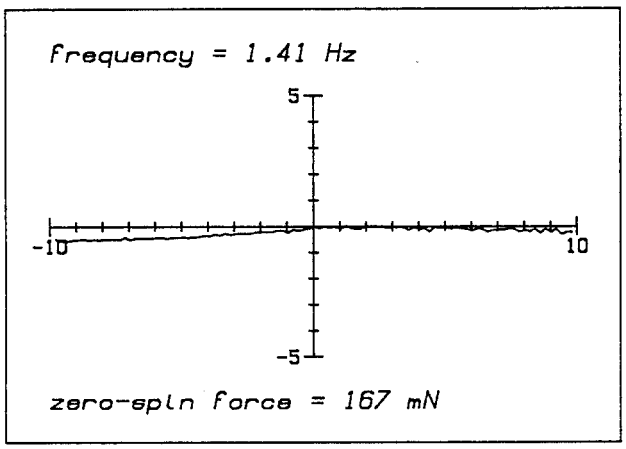

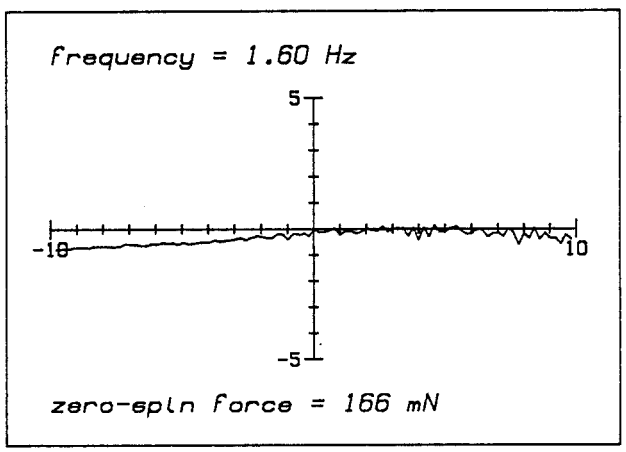

Wave amplitude

Considering heave and surge in-phase force:

1) The central region of the graph changes considerably with amplitude. At 5 mm its slope is barely distinguishable from the rest of the graph. At higher amplitudes it increases, and a distinct 'knee' forms in the curve in both the positive and negative spin regions as, at a point usually around spin factor 1, the slope changes to a lower value. The slope of the central region appears to be greatest for amplitudes 15 - 20 mm. For higher amplitudes still, the slope of the central region abruptly drops, and the high-slope part of the curve is pushed out to larger spin factors, so that a double knee now appears in both the positive and negative spin regions. These effects occur in both heave and surge, albeit more pronounced in heave.

2) The zero-spin force does not rise smoothly with wave amplitude. It shows a pronounced dip around the 15 - 20 mm region.

3) By contrast, the force factor curves are steepest around the 15 - 20 mm region. The effect is greater for heave than surge.

Considering heave and surge quadrature forces:

4) For 5 and 10 mm amplitudes, the curves follow the expected pattern, namely, zero or small force factor with positive spin, and a steady change with negative spin.

5) For higher amplitudes the curves change a lot. More and more quadrature force appears at high positive and negative spin. It is comparable to the in-phase force, indicating that the angle of total force is very different from the angle of the zero-spin force. Clearly the drag and inertial forces are changing their ratio. One would expect this, because the inertial forces are proportional to the water velocity while the drag forces are proportional to its square.

6) The double knee effect in the in-phase graphs does not appear here, but for the 25 mm amplitude graph, between spin factor -1 and -3, the curve actually reverses its slope. Interestingly, the quadrature curves are much smoother than the in-phase ones.

Figure 3a IN-PHASE HEAVE force factor against spin factor

6 WAVE AMPLITUDES

Wave frequency = 1.02 Hz

Cylinder depth = 100 mm

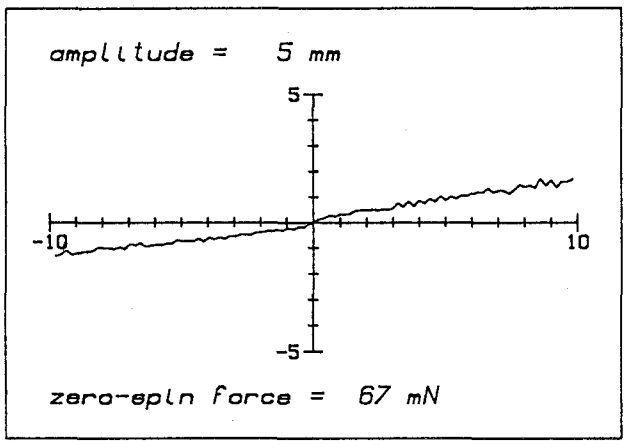

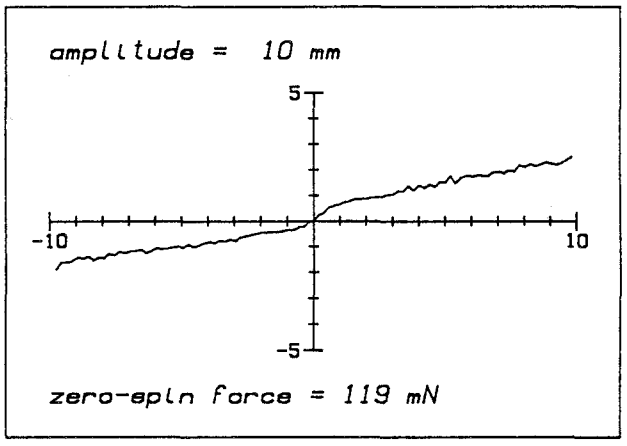

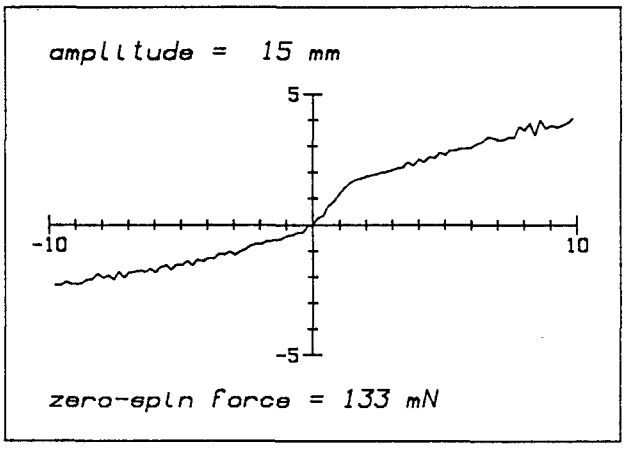

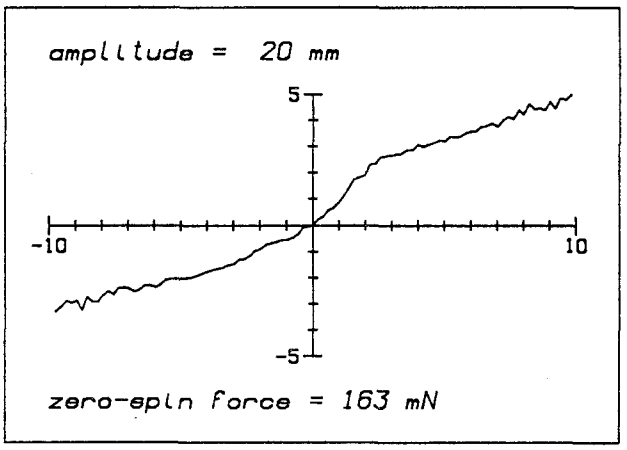

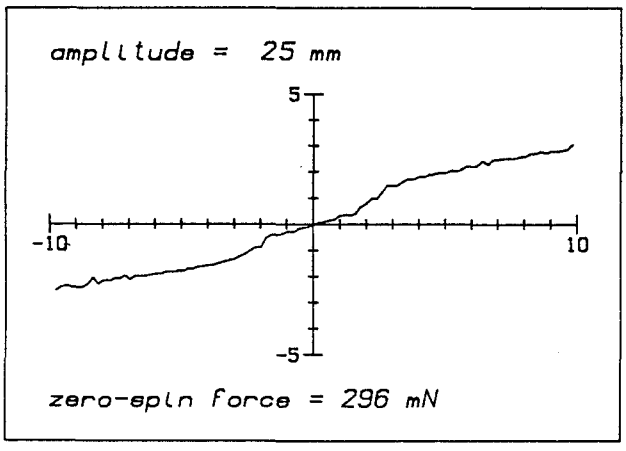

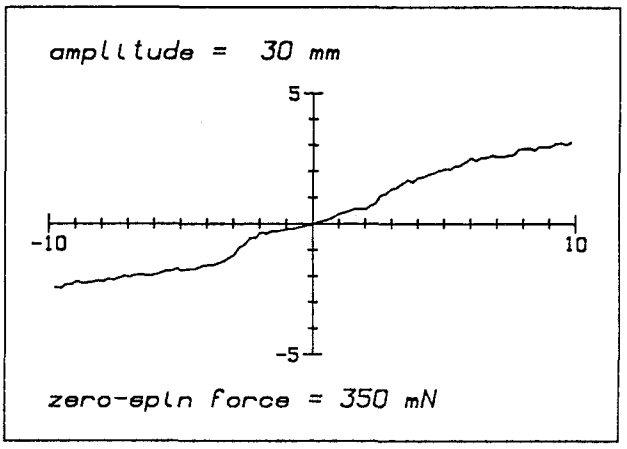

Figure 3b QUADRATURE HEAVE force factor against spin factor

Wave frequency = 1.02 Hz

6 WAVE AMPLITUDES

Cylinder depth = 100 mm

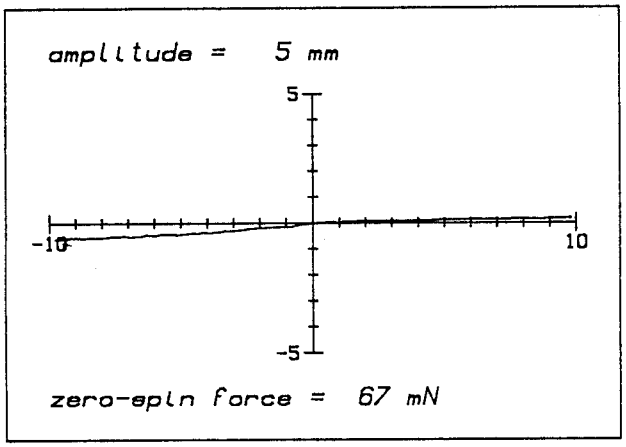

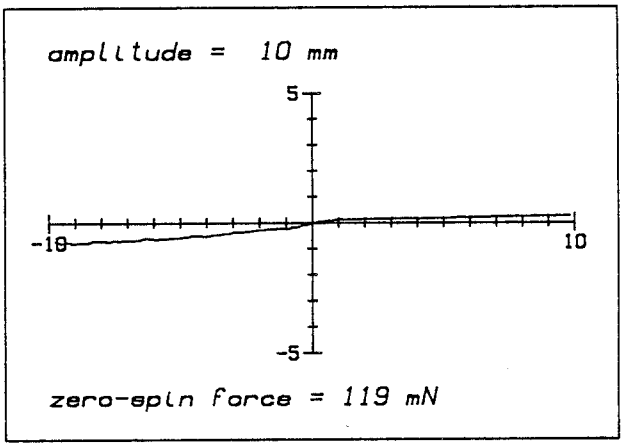

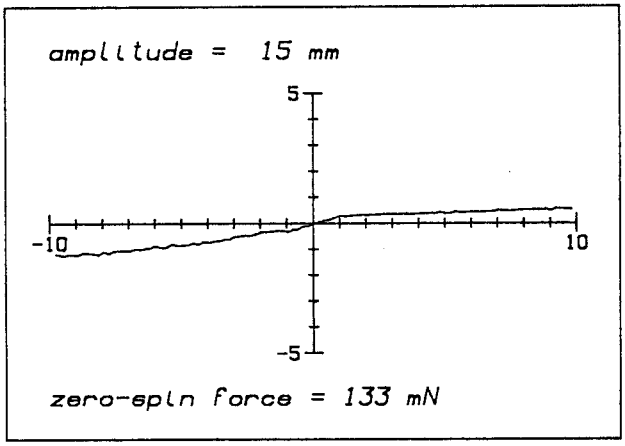

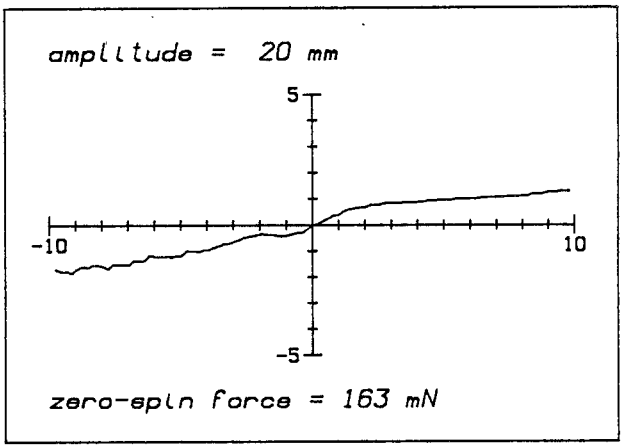

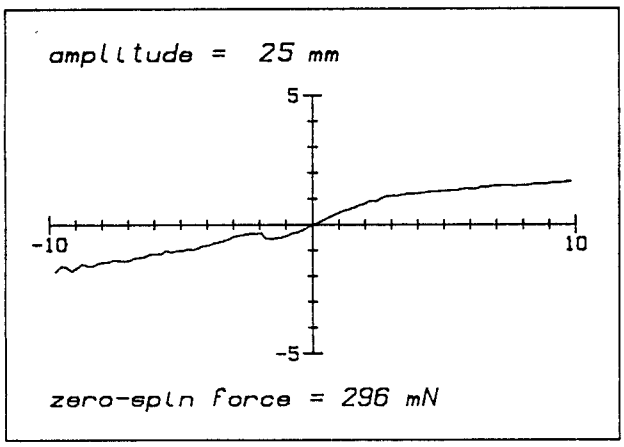

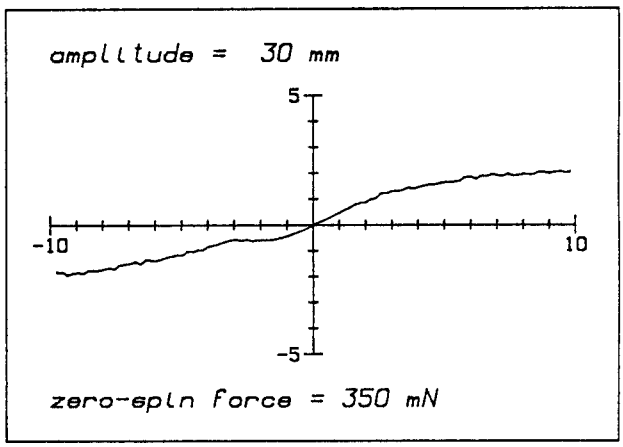

Figure 3c IN-PHASE SURGE force factor against spin factor

6 WAVE AMPLITUDES

Wave frequency = 1.02 Hz

Cylinder depth = 100 mm

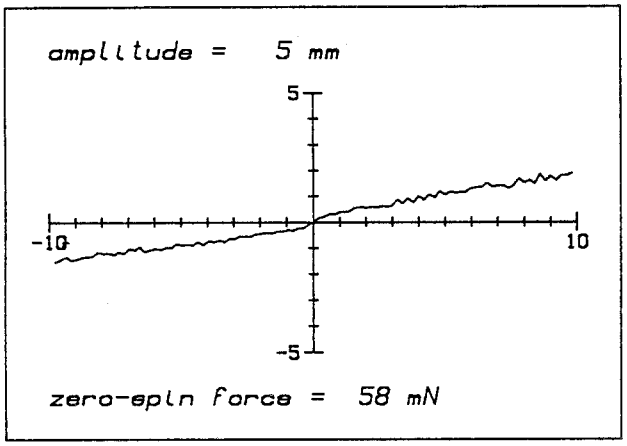

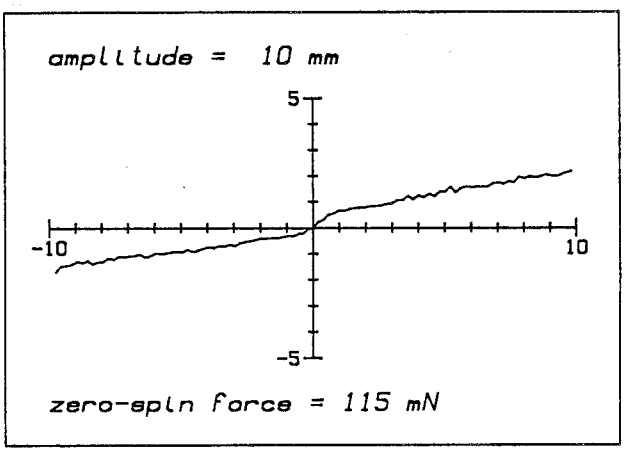

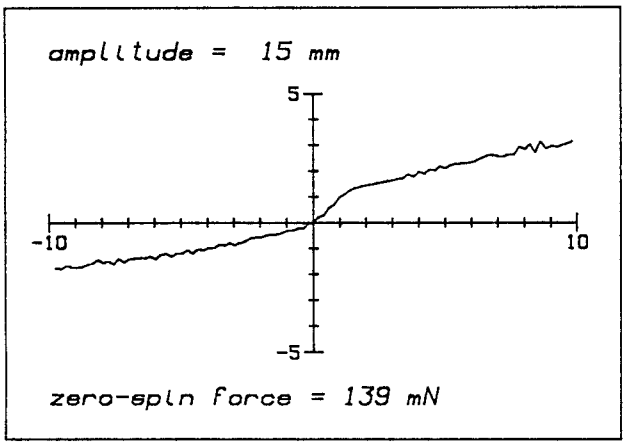

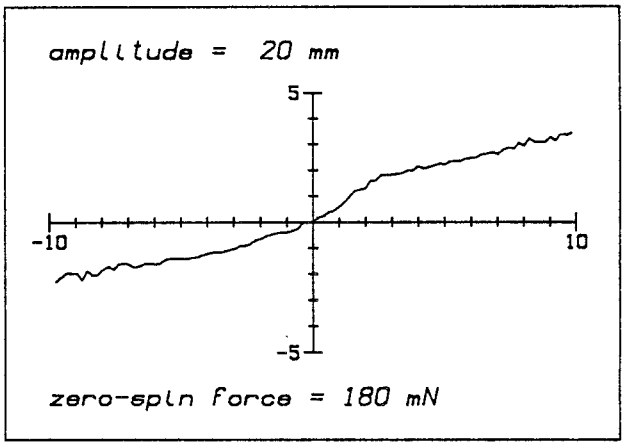

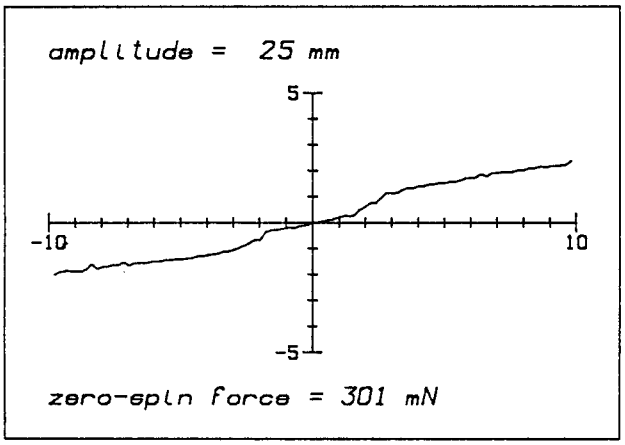

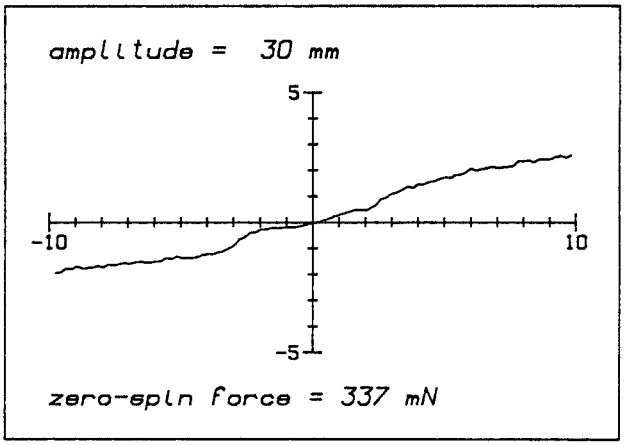

Figure 3d QUADRATURE SURGE force factor against spin factor

Wave frequency = 1.02 Hz

6 WAVE AMPLITUDES

Cylinder depth = 100 mm

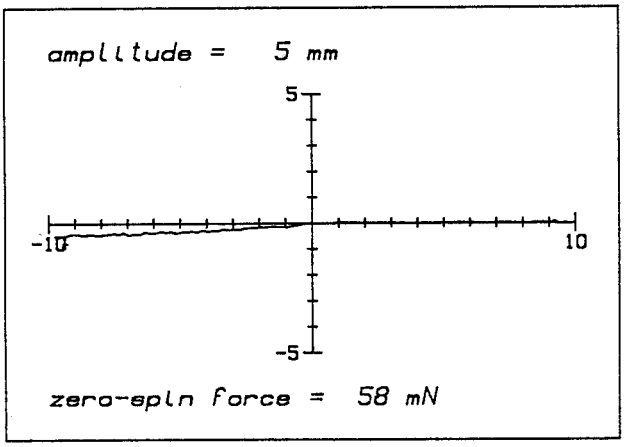

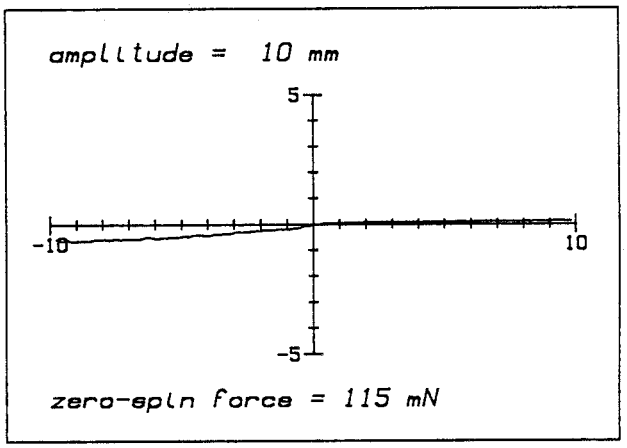

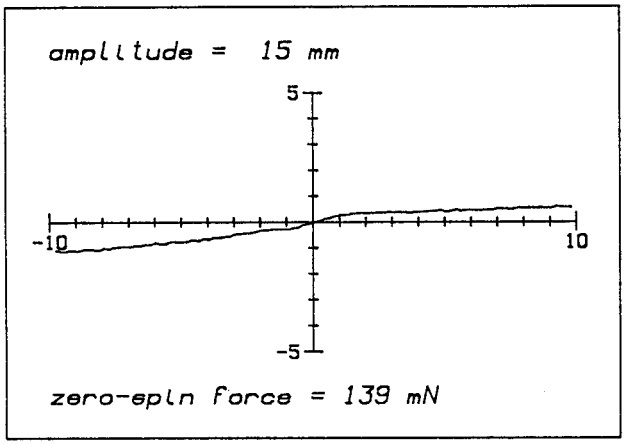

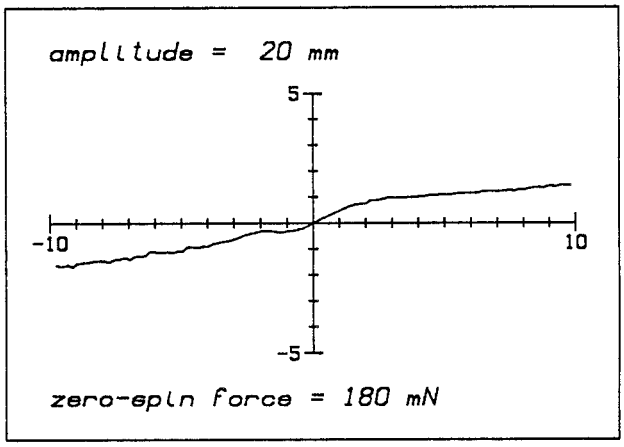

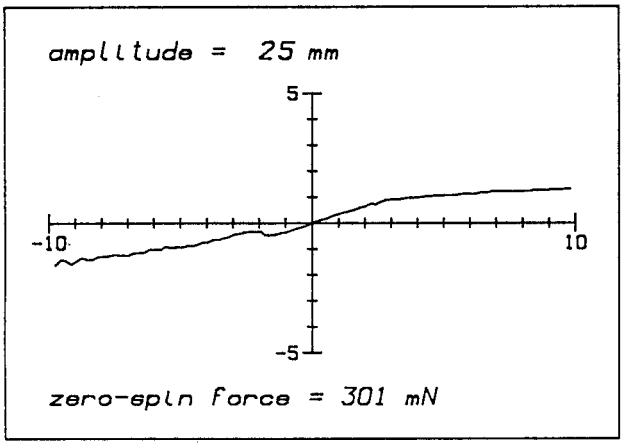

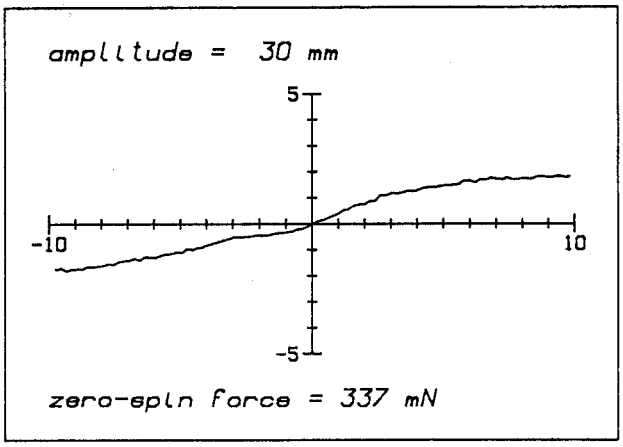

THE TABLES

The following tables provide a summary of the previous graphs for in-phase heave and surge force. The parameter under test (depth, frequency, amplitude) is presented in the top row, and the columns beneath pertain to the stated values of this parameter. In the fourth row is the calculated force on the rest cylinder, and in the fifth is the measured force on the rest cylinder.

The force on the rest cylinder is calculated from the Morison equation:

1) $$F = \rho \pi r^2 L C_m \frac{dU}{dt} + \rho r L C_d U|U|$$

inertial force drag force

U = fluid velocity
ρ = density of water
r = cylinder radius
L = cylinder length
C_m = inertial coefficient
C_d = drag coefficient

For periodic waves we can rewrite this as:

2) $$F = \rho \pi r^2 L C_m \omega^2 a + \rho r L C_d (\omega a)^2$$

ω = angular frequency of the wave

where a is the amplitude of the wave at the submergence of the cylinder. For a wave in water of finite depth, the heave and surge amplitudes are:

3) $$\text{heave amplitude at depth d} = \frac{A \sinh k(h-d)}{\sinh kh}$$

4) $$\text{surge amplitude at depth d} = \frac{A \cosh k(h-d)}{\sinh kh}$$

$k = 2\pi/\text{wavelength}$
h = water depth
A = surface amplitude

Values of C_m and C_d for Morison's equation are determined empirically. For a deeply submerged horizontal cylinder Chaplin (1984) offers the expression:

5) $$C_m = 2 - 0.21K_c^2$$

K_c = Keulegan-Carpenter number

noting that it cannot be used beyond $K_c = 2$ because of vortex-shedding effects. C_d also varies with scale. We used a constant value of 1, justifiable because the drag component changed the resultant force by less than 2% in all cases.

The 'SF +10 force' is the additional force experienced at spin factor +10.
The 'SF -10 force' is that experienced at spin factor -10.
The '+/- force ratio' is the magnitude of the ratio of those two forces.

Table 1a CYLINDER FORCE WITH CYLINDER DEPTH

Wave frequency 1.02 Hz, wave amplitude 10 mm

HEAVE

Depth	mm	40	60	80	100	120	140
Local wave amplitude	mm	8.44	7.76	7.12	6.53	5.99	5.49
Keulegan-Carpenter number		1.56	1.43	1.32	1.21	1.11	1.02
Inertial coefficient		1.49	1.57	1.64	1.69	1.74	1.78
Morison force	mN	136	131	125	119	112	105
Zero-spin force	mN	143	133	120	114	116	118
SF +10 force	mN	393	426	350	302	257	236
SF -10 force	mN	-197	-208	-211	-191	-188	-176
SF +10 force factor		2.7	3.2	2.9	2.6	2.2	2.0
SF -10 force factor		-1.4	-1.6	-1.8	-1.7	-1.6	-1.5
+/- force ratio		2.0	2.0	1.7	1.6	1.4	1.3

SURGE

Depth	mm	40	60	80	100	120	140
Local wave amplitude	mm	8.64	7.97	7.35	6.78	6.26	5.79
Keulegan-Carpenter number		1.60	1.47	1.36	1.25	1.16	1.07
Inertial coefficient		1.46	1.54	1.61	1.67	1.72	1.76
Morison force	mN	136	133	128	122	116	109
Zero-spin force	mN	137	131	119	111	111	106
SF +10 force	mN	305	370	311	266	226	196
SF -10 force	mN	-211	-198	-192	-167	-160	-139
SF +10 force factor		2.2	2.8	2.6	2.4	2.0	1.8
SF -10 force factor		-1.5	-1.5	-1.6	-1.5	-1.4	-1.3
+/- force ratio		1.4	1.9	1.6	1.6	1.4	1.4

Table 2a CYLINDER FORCE WITH WAVE FREQUENCY

Cylinder depth 100 mm, wave amplitude 10 mm

HEAVE

Frequency	Hz	0.63	0.82	1.02	1.21	1.41	1.60
Local wave amplitude	mm	7.94	7.38	6.53	5.53	4.51	3.56
Keulegan-Carpenter number		1.47	1.36	1.21	1.02	0.83	0.66
Inertial coefficient		---	1.61	1.69	1.78	1.85	1.91
Morison force	mN	---	83	119	150	172	182
Zero-spin force	mN	31	81	120	146	173	189
SF +10 force	mN	182	218	291	334	356	308
SF -10 force	mN	-121	-144	-202	-226	-253	-250
SF +10 force factor		5.7	2.7	2.4	2.3	2.1	1.6
SF -10 force factor		-3.8	-1.8	-1.7	-1.5	-1.5	-1.3
+/- force ratio		1.5	1.5	1.4	1.5	1.4	1.2

SURGE

Frequency	Hz	0.63	0.82	1.02	1.21	1.41	1.60
Local wave amplitude	mm	12.4	8.57	6.78	5.57	4.52	3.56
Keulegan-Carpenter number		2.30	1.58	1.25	1.03	0.83	0.66
Inertial coefficient		---	1.47	1.67	1.78	1.85	1.91
Morison force	mN	---	89	122	151	172	182
Zero-spin force	mN	68	81	118	137	167	166
SF +10 force	mN	133	206	260	293	302	287
SF -10 force	mN	- 86	-142	-179	-192	-211	-212
SF +10 force factor		1.9	2.5	2.2	2.1	1.8	1.7
SF -10 force factor		-1.3	-1.7	-1.5	-1.4	-1.3	-1.3
+/- force ratio		1.5	1.5	1.5	1.5	1.4	1.4

Table 3a CYLINDER FORCE WITH WAVE AMPLITUDE

Cylinder depth 100 mm, wave frequency 1.02 Hz

HEAVE

Surface wave amplitude	mm	5	10	15	20	25	30
Local wave amplitude	mm	3.27	6.53	9.80	13.0	16.3	19.6
Keulegan-Carpenter number		0.60	1.21	1.81	2.42	3.02	3.62
Inertial coefficient		1.92	1.69	1.31	---	---	---
Morison force	mN	67	119	139	---	---	---
Zero-spin force	mN	67	119	133	163	296	350
SF +10 force	mN	117	301	554	824	908	1149
SF -10 force	mN	- 86	-201	-319	-530	-746	-859
SF +10 force factor		1.7	2.5	4.1	5.0	3.1	3.3
SF -10 force factor		-1.3	-1.7	-2.4	-3.2	-2.5	-2.5
+/- force ratio		1.4	1.5	1.7	1.6	1.2	1.3

SURGE

Surface wave amplitude	mm	5	10	15	20	25	30
Local wave amplitude	mm	3.39	6.78	10.2	13.6	17.0	20.4
Keulegan-Carpenter number		0.63	1.25	1.88	2.51	3.13	3.76
Inertial coefficient		1.92	1.67	1.26	---	---	---
Morison force	mN	70	122	139	---	---	---
Zero-spin force	mN	58	115	139	180	301	337
SF +10 force	mN	111	259	452	635	720	915
SF -10 force	mN	- 87	-175	-255	-399	-594	-644
SF +10 force factor		1.9	2.2	3.2	3.5	2.4	2.7
SF -10 force factor		-1.5	-1.5	-1.8	-2.2	-2.0	-1.9
+/- force ratio		1.3	1.5	1.8	1.6	1.2	1.4

THE LIFT FORCE

Budal, in his derivation (1985) assumes waves in water of infinite depth and hence makes no distinction between heave and surge displacement of water particles. However, under shallow water test conditions, there will indeed be a difference. As Budal makes clear, the additional force is a Magnus lift effect due to the fluid velocity at right-angles to the fluid acceleration. Consequently, rather than relating the lift force to the inertial force on the rest cylinder, it makes more sense to relate it to the fluid velocity at right-angles to the force. Because we are not equipped to measure the complete velocity field in the presence of the cylinder we approximate it by using the standard equation for unobstructed flow.

This has been done in the following tables. The heave (or surge) force on the cylinder at +10 and -10 spin factors has been reprinted from the previous set of tables. Below that is shown the surge (or heave) fluid velocity appropriate to the test conditions calculated from equations (3) and (4). The quotient of force and velocity is printed below that.

In the case of frequency, there are additional rows in which these force/velocity coefficients have been divided by frequency. The result is a new coefficient showing much less variation across the frequency range, implying that the Budal force is - at least at these high spin values - better related to spin rate than to spin factor.

For all the experiments, this new force coefficient shows considerably less variation with depth, amplitude, or frequency than the force factors of the first set of tables. In particular, the egregiously high positive force factor in heave in the 0.63 Hz wave disappears. The variations which remain can be used more confidently as indicators of real physical effects. The heave and surge, positive and negative force factors, for variation in any given parameter, all tend to follow the same trend. For example, with depth, a maximum in the force factors appears at 60 mm - about three and a half cylinder radii. With wave amplitude there is also a distinct maximum in the force factors at 20 mm amplitude - ie, comparable with the cylinder radius. This is the point at which water orbitals are just able to envelop the cylinder. With frequency, there is a general trend for the force factor to decrease as frequency increases. An exception to the trend for the force factors to change in sympathy with each other is the negative surge force factor with depth, which shows no significant change as depth increases.

Table 1b CYLINDER FORCE AND FLUID VELOCITY WITH CYLINDER DEPTH

Wave frequency 1.02 Hz, wave amplitude 10 mm

HEAVE

Depth	mm	40	60	80	100	120	140
Heave SF +10 force	mN	393	426	350	302	257	236
Heave SF -10 force	mN	-197	-208	-211	-191	-188	-176
Surge fluid velocity	mm/s	55.1	50.8	46.9	43.3	40.0	36.9
SF +10 force/velocity	Ns/m	7.1	8.4	7.5	7.0	6.4	6.4
SF -10 force/velocity	Ns/m	-3.6	-4.1	-4.5	-4.4	-4.7	-4.8

SURGE

Depth	mm	40	60	80	100	120	140
Surge SF +10 force	mN	305	370	311	266	226	196
Surge SF -10 force	mN	-211	-198	-192	-167	-160	-139
Heave fluid velocity	mm/s	53.9	49.5	45.4	41.7	38.2	35.1
SF +10 force/velocity	Ns/m	5.7	7.5	6.9	6.4	5.9	5.6
SF -10 force/velocity	Ns/m	-3.9	-4.0	-4.2	-4.0	-4.2	-4.0

Table 2b CYLINDER FORCE AND FLUID VELOCITY WITH WAVE FREQUENCY

Cylinder depth 100 mm, wave amplitude 10 mm

HEAVE

Frequency	Hz	0.63	0.82	1.02	1.21	1.41	1.60
Heave SF +10 force	mN	182	218	291	334	356	308
Heave SF -10 force	mN	-121	-144	-202	-226	-253	-250
Surge fluid velocity	mm/s	48.9	44.2	43.3	42.4	39.9	35.9
SF +10 force/velocity	Ns/m	3.7	4.9	6.7	7.9	8.9	8.6
SF -10 force/velocity	Ns/m	-2.5	-3.3	-4.7	-5.3	-6.3	-7.0
SF +10 force/vel/freq	N/m	5.9	6.0	6.7	6.5	6.3	5.4
SF -10 force/vel/freq	N/m	-3.9	-4.0	-4.7	-4.4	-4.5	-4.4

SURGE

Frequency	Hz	0.63	0.82	1.02	1.21	1.41	1.60
Surge SF +10 force	mN	133	206	260	293	302	287
Surge SF -10 force	mN	- 86	-142	-179	-192	-211	-212
Heave fluid velocity	mm/s	31.2	38.0	41.7	42.1	39.9	35.9
SF +10 force/velocity	Ns/m	4.3	5.4	6.2	7.0	7.6	8.0
SF -10 force/velocity	Ns/m	-2.8	-3.7	-4.3	-4.6	-5.3	-5.9
SF +10 force/vel/freq	N/m	6.8	6.6	6.2	5.8	5.4	5.0
SF -10 force/vel/freq	N/m	-4.4	-4.6	-4.3	-3.8	-3.8	-3.7

Table 3b CYLINDER FORCE AND FLUID VELOCITY WITH WAVE AMPLITUDE

Cylinder depth 100 mm, wave frequency 1.02 Hz

HEAVE

Amplitude	mm	5	10	15	20	25	30
Heave SF +10 force	mN	117	301	554	824	908	1149
Heave SF -10 force	mN	- 86	-201	-319	-530	-746	-859
Surge fluid velocity	mm/s	21.6	43.3	64.9	86.6	108.2	129.8
SF +10 force/velocity	Ns/m	5.4	7.0	8.5	9.5	8.4	8.9
SF -10 force/velocity	Ns/m	-4.0	-4.6	-4.9	-6.1	-6.9	-6.6

SURGE

Amplitude	mm	5	10	15	20	25	30
Surge SF +10 force	mN	111	259	452	635	720	915
Surge SF -10 force	mN	- 87	-175	-255	-399	-594	-644
Heave fluid velocity	mm/s	20.8	41.7	62.5	83.4	104.2	125.1
SF +10 force/velocity	Ns/m	5.3	6.2	7.2	7.6	6.9	7.3
SF -10 force/velocity	Ns/m	-4.2	-4.2	-4.1	-4.8	-5.7	-5.1

WAVE MEASUREMENTS

In each of the three experiments we recorded the wave gauge outputs. We then repeated the experiments without the cylinder. The gauges were separated by 1.2 metres and their signals show a phase difference which is of course dependent on frequency. This phase difference is also affected by the presence of the cylinder, and by whether it is spinning or not. In the following graphs, the phase change due to the presence of the cylinder is plotted against spin factor. All of the graphs show some dependence on spin.

We ran a repeatablity experiment to check the reliability of the phase measurements. Shown below is the root-mean-square phase error with frequency. This was the rms deviation from the mean phase difference between the fore and aft wave gauges with no cylinder present.

Frequency	Hz	0.63	0.82	1.02	1.21	1.41	1.60
Rms phase error	degrees	0.06	0.07	0.06	0.10	0.25	1.53

These low levels of error allow confidence in the phase measurement technique. However, the rapid rise of error at 1.6 Hz should be noted. This is due to a cross-wave in the tank, the lowest frequency at which such a resonance occurs.

Ogilvie (1963) derived the phase of force on a submerged fixed cylinder due to waves. He also indicated the phase lag in the wave that the presence of the cylinder causes at the surface. For a fixed wave frequency it increases with cylinder size and proximity to the surface.

Mehlum (1980) offered a new approach which allows an economical computation of the phase lag. He included graphs of phase lag against cylinder and wave parameters. Unfortunately they are plotted only for large values. A program of ours using Mehlum's algorithm was checked against his graphs, then used to calculate the phase lags due to our much smaller cylinder, when at zero spin. These values are compared with the measured results in the comments for each graph.

Over the spin range tested, spinning the cylinder produced phase changes several times the phase change due to the fixed cylinder. Moreover, there were interesting correlations with the force graphs in all three experiments. The larger the forces, the greater the phase change. And where the force graphs showed force cancellation, the wave phase change approached zero.

Cylinder Depth

1) The graphs are linear with spin, for depths of 60 mm and more.

2) The slope of the line - which is the measure of the effect of spin on phase lag - decreases with depth.

3) Below is a table of the measured phase lag caused by the cylinder when at rest, compared with the theoretical lag calculated by Mehlum's algorithm.

Depth	mm	40	60	80	100	120	140
Theoretical lag	deg	2.7	2.2	1.9	1.6	1.3	1.1
Measured lag	deg	3.0	2.8	2.2	2.1	2.0	1.9

While the trend is similar, agreement is only fair. It would be useful to check these data again, using instead of a pair of gauges a pair of wave-gauge arrays to give better resolution of phase.

Figure 1e WAVE PHASE CHANGE IN DEGREES AGAINST SPIN FACTOR

6 CYLINDER DEPTHS

Wave frequency = 1.02 Hz

Wave amplitude = 10 mm

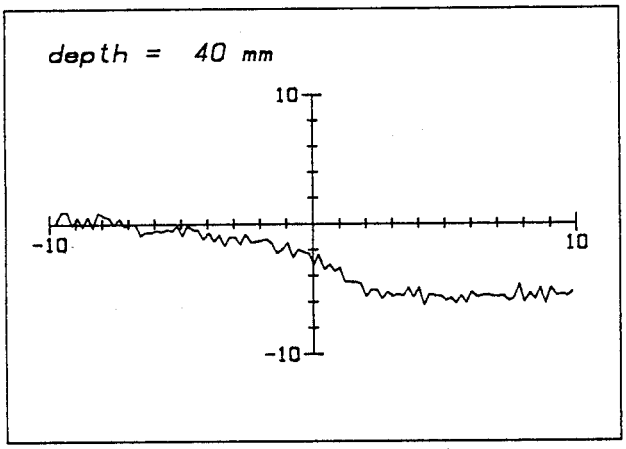

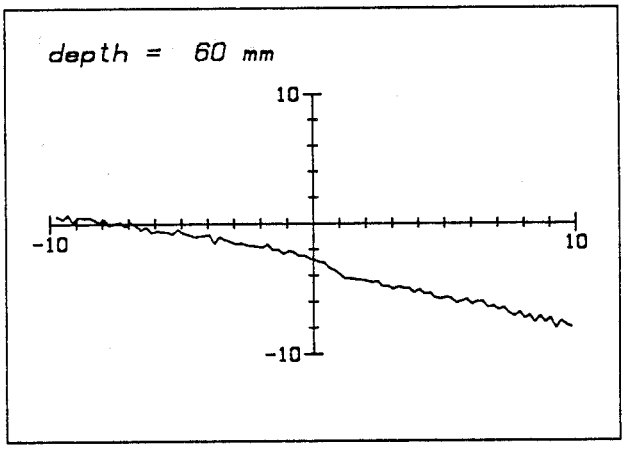

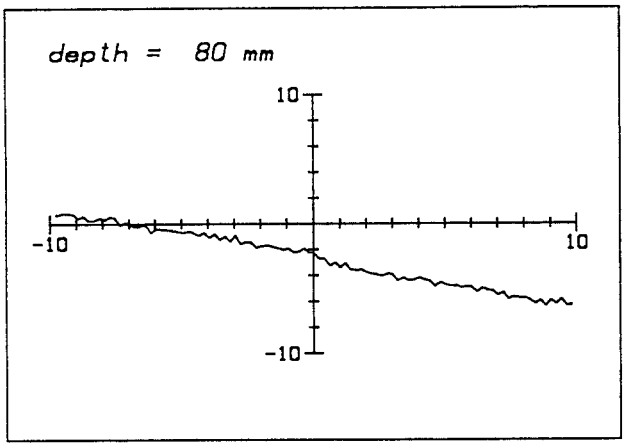

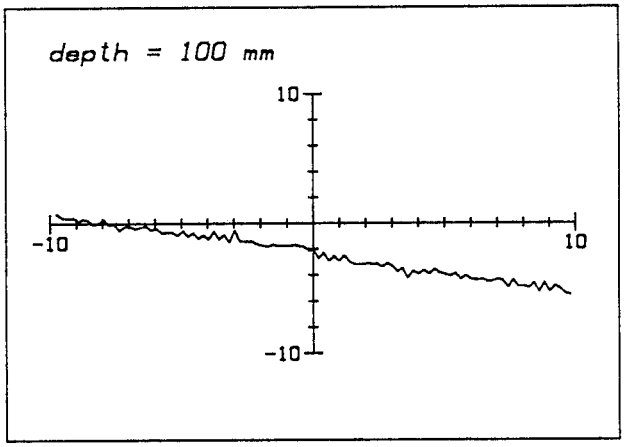

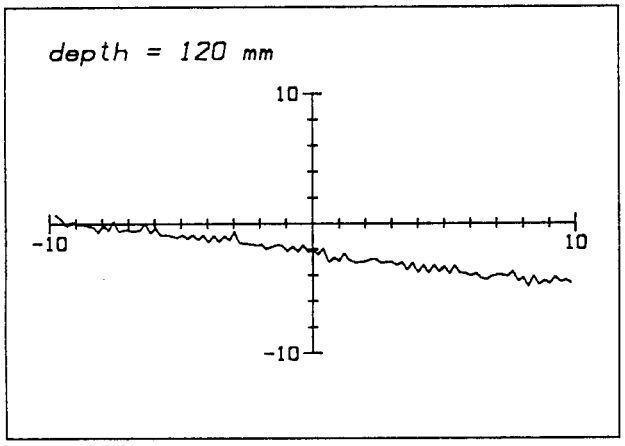

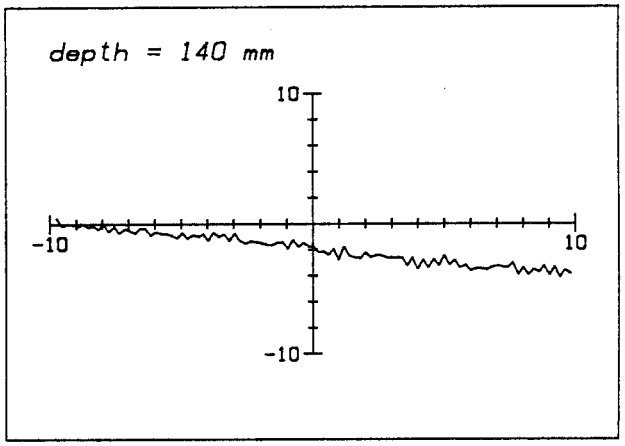

Wave frequencies

1) In each graph phase lag increases linearly with spin factor.

2) The change with frequency is very marked. The slope of the line is proportional to frequency cubed (see table below). Because the horizontal axis is spin factor, we can deduce that the slope of the line of phase lag against cylinder angular velocity is proportional to frequency squared. Since wavelength is also proportional to frequency squared, this is equivalent to saying that, at any frequency, the lag as a fraction of wavelength is proportional to spin speed.

3) The phase lag due to the rest cylinder also increases with frequency, in fact at a rate greater than that predicted by theory. See table.

frequency	Hz	0.63	0.82	1.02	1.21	1.41	1.60
theoretical lag	deg	0.4	0.9	1.6	2.3	2.7	2.8
measured lag	deg	1.0	0.5	2.0	3.0	5.0	7.0
graph slope		0.08	0.15	0.31	0.57	0.88	1.46
slope/freq cubed		0.32	0.27	0.29	0.32	0.31	0.35

Figure 2e WAVE PHASE CHANGE IN DEGREES AGAINST SPIN FACTOR

Wave amplitude = 10 mm

6 WAVE FREQUENCIES

Cylinder depth = 100 mm

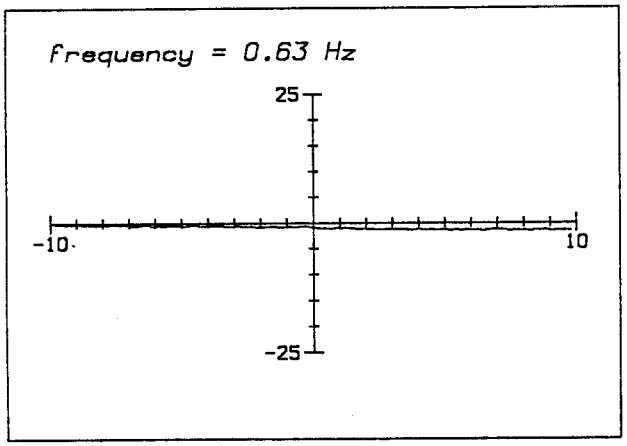

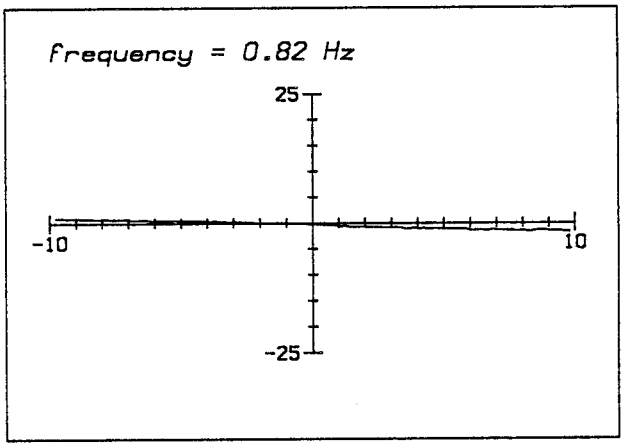

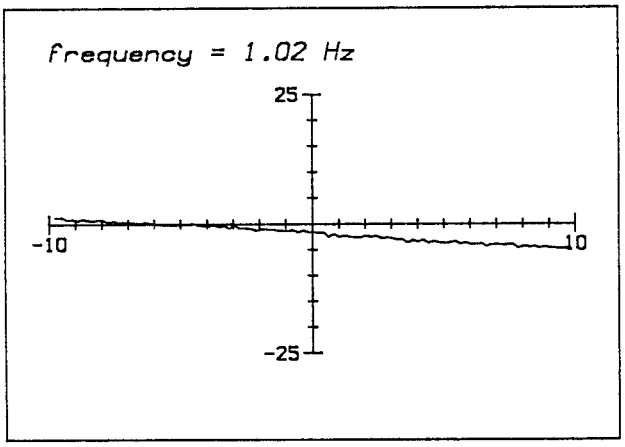

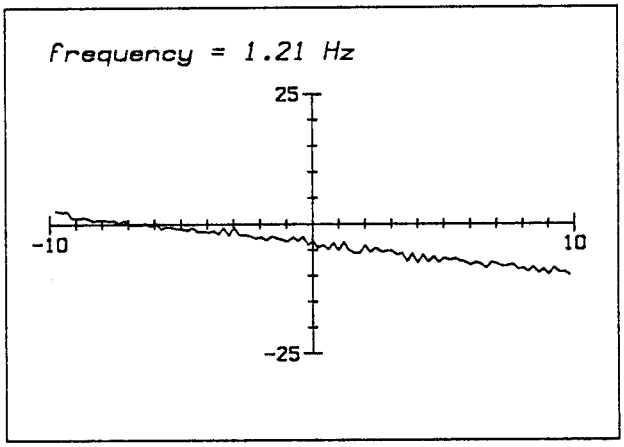

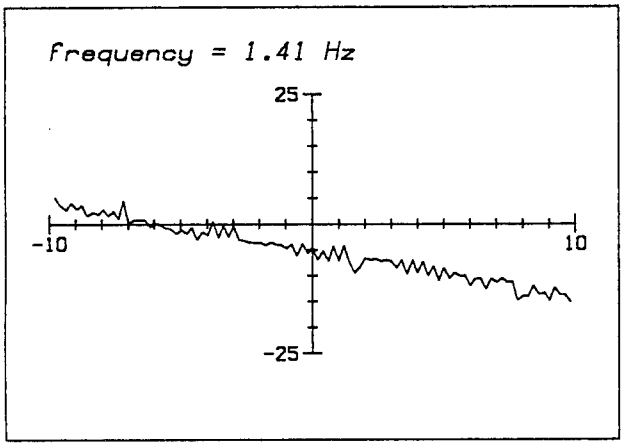

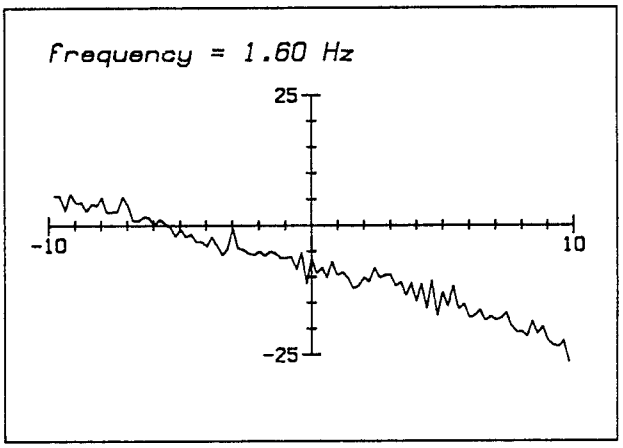

Wave amplitude

1) The theoretical phase lag for the rest cylinder is 1.6 degrees. The measured lag agrees with this quite closely until the amplitude reaches 30 mm.

2) Phase lag is linearly proportional to spin factor until the amplitude reaches 25 mm.

Figure 3e WAVE PHASE CHANGE IN DEGREES AGAINST SPIN FACTOR

Wave frequency = 1.02 Hz

6 WAVE AMPLITUDES

Cylinder depth = 100 mm

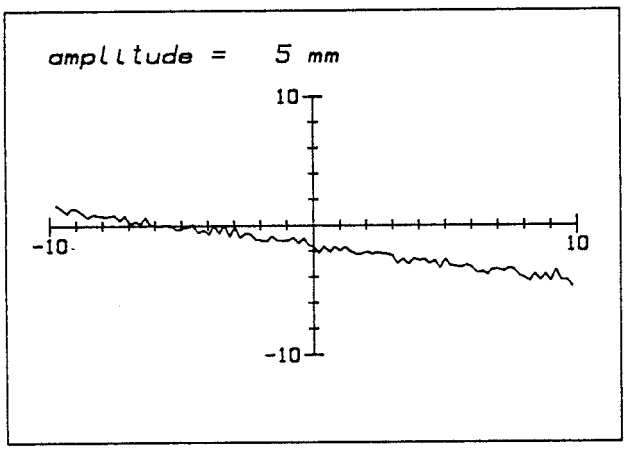

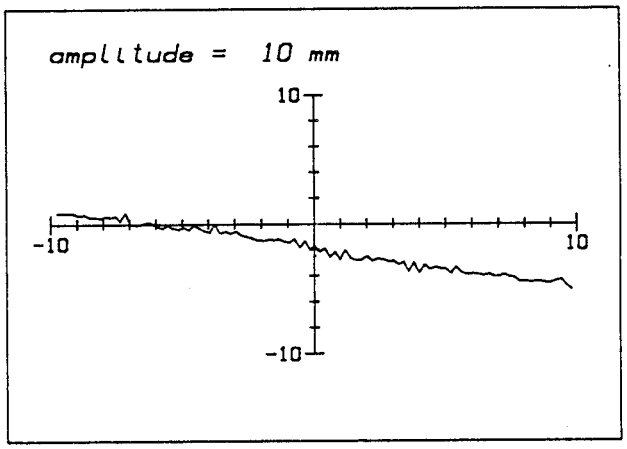

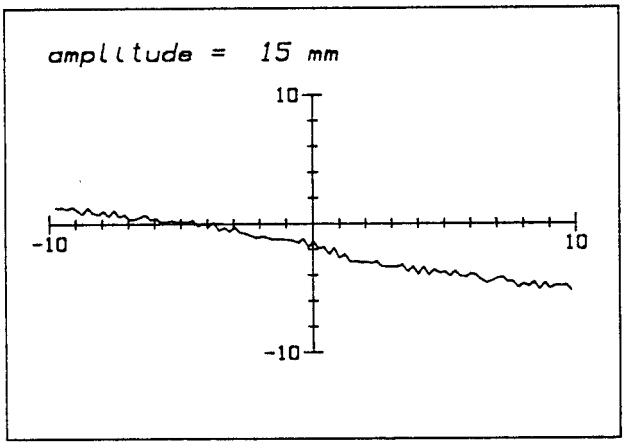

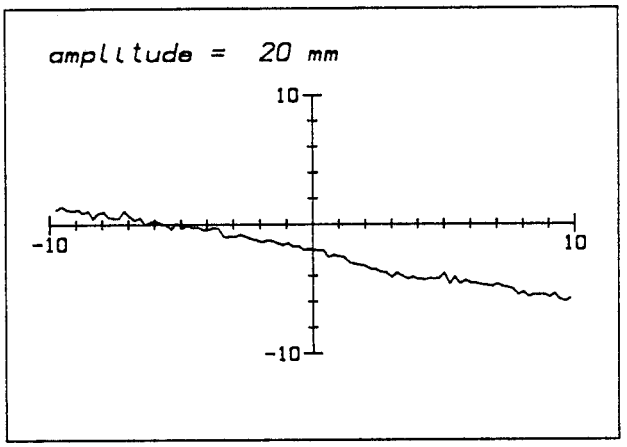

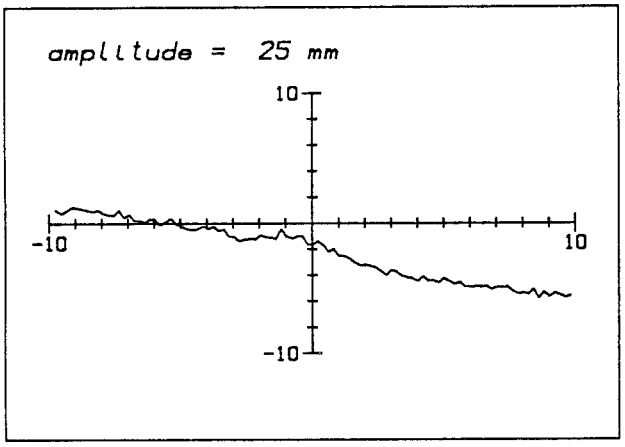

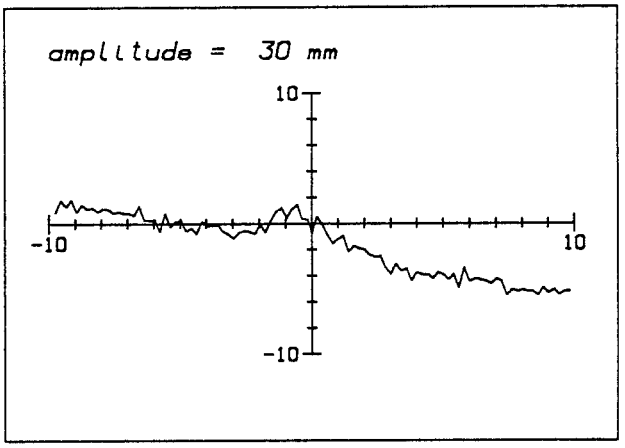

REFERENCES

Budal K, Lillebekken P M (1985) Wave forces on a horizontal submerged spinning cylinder. Hydrodynamics of Ocean Wave-Energy Symposium, IUTAM Symposium Lisbon.

Chaplin J R (1984) Non-linear forces on a horizontal cylinder beneath waves. Journal of Fluid Mechanics v 147 p 449

Coutanceau M, Menard C (1985) Influence of rotation on the near-wake development behind an impulsively started circular cylinder. Journal of Fluid Mechanics v 158 p 399

Mehlum E (1980) A circular cylinder in water waves. Applied Ocean Research v 2 no. 4

APPENDIX 1 THE LOAD CELL SPECIFICATION

****

R.S. COMPONENTS

CALIBRATION ACCEPTANCE CERTIFICATE

****

Calibration mode:-	Compression	Serial number	88710m
Input impedance	415 Ohms	Model	505H
Output impedance	350 Ohms	Capacity (kg)	2
Insulation resistance >	5 Gohms	Grade	D2
Test excitation	10 Vdc	Accuracy	0.05%
Max. excitation	15 Vdc	Part Number	632 736

Zero balance	+0.28	% Rated load
Output rated load	+2.19	mV/V

Total error(#1)	0.025	% Rated load
Nonrepeatability	0.010	% Rated load
Creep/zero return(#2)	0.005	% Rated load
Eccentricity(#3)	0.005	% Rated load

Eccentricity test load	1 kg.
Platform size	150 x 150 m.m.'s

Temperature effect
****

on zero balance	0.0075	% Rated load/10 deg C
on output (span)	< 0.0150	% Rated load/10 deg C

Compensated temperature range	-10 to +50 deg C
Safe temperature range	-30 to +70 deg C

****

#1 Total error is the maximum deviation from a straight line drawn between the no load and rated load outputs for both increasing and decreasing loads.

#2 Both creep and zero return are measured, using rated load, and the worst result is used for accuracy classification.

#3 Eccentricty is the max. deviation from the output at the centre when the test load is placed anywhere else on the platform.

****

Cable colour code
****

Green = +Excitation	Blue = +Sense	Red = +Output
Black = -Excitation	Yellow = -Sense	White = -Output

****

Manufactured for:-

R.S. Components
P.O. Box 99
Birchington Road
Weldon
Corby NN17 9RS
United Kingdom
Tel.(0536) 201234
Tlx.342512

Q.A. release 2 418as6330n